

# Thermodynamics of Quantum Coupled Transport

Shuvadip Ghosh<sup>1,\*</sup> and Arnab Ghosh<sup>1,†</sup>

<sup>1</sup>*Indian Institute of Technology Kanpur, Kanpur, Uttar Pradesh 208016, India*

(Dated: March 9, 2026)

This review presents a comprehensive thermodynamic perspective on quantum coupled transport processes in nanoscale systems. Our analysis is formulated within the framework of entropy production rate, the central thermodynamic quantity that governs non-equilibrium processes and can be expressed in terms of the existing conjugate force–flux pairs. Although thermodynamic laws are valid across classical–quantum boundaries, our analysis is carried out within a microscopic open quantum system framework, focusing on quantum dots (QDs) coupled to electronic reservoirs. We begin with elementary single transport processes and highlight their strong thermodynamic constraints in the near-equilibrium regime. This motivates the study of coupled transport, where multiple force–flux pairs coexist and interact, giving rise to richer thermodynamic behaviour. Employing the entropy production rate as the guiding principle, we analyse coupled energy and particle transport in a minimal two-terminal single–QD setup and show how standard thermoelectric phenomena, such as Seebeck and Peltier effects, as well as thermoelectric heat engines and refrigerators, naturally emerge as a consequence of thermodynamic cross-effects. Next, we extend the framework to a three-terminal coupled quantum dot (CQD) geometry, which provides a versatile platform for exploring coupled transport. Under appropriate constraints, this model reduces to the well-known Sánchez–Büttiker configuration, capturing conventional thermoelectric behaviour analogous to that of classical devices. Beyond standard cross-effects, we focus on the conceptually distinct and counter-intuitive phenomenon of inverse currents in coupled transport (ICC), where a current flows against all mutually parallel thermodynamic forces without violating the second law of thermodynamics. We demonstrate that genuine ICC requires breaking the symmetry between energy and particle transport and identify the necessary and sufficient conditions for its realisation within a reduced CQD framework through attractive interdot interactions. Finally, we discuss the implications of the ICC for the design of autonomous quantum thermoelectric engines and refrigerators, highlighting new avenues for unconventional thermodynamic functionality in QD-based systems.

## I. INTRODUCTION

*“Thermodynamics is the only physical theory of universal content which I am convinced that, within the framework of applicability of its basic concepts, will never be overthrown.”* — ALBERT EINSTEIN

This celebrated remark by *Albert Einstein* eloquently underscores the fundamental and universal character of thermodynamics. Unlike many physical theories whose validity is limited by scale, approximation, or domain of applicability, thermodynamics transcends the classical–quantum boundary *per se* [1–4] and remains relevant across an exceptionally broad spectrum of physical systems. Adopting a thermodynamic perspective to analyse physical processes is, therefore, not only natural but also deeply insightful. Such an approach is often illuminating and reveals model-independent information and governing principles, thereby opening rich avenues for both theoretical exploration and experimental investigation.

In this review, we focus on the thermodynamic aspects of a particular class of transport phenomena, namely coupled quantum transport processes. Transport phenomena themselves constitute an extensively studied area of research [5, 6], with a vast literature that includes both

classical [7] and quantum systems [8]. Although classical and quantum transport differ fundamentally in their microscopic mechanisms and mathematical formalisms [9], the present work does not aim to address these detailed dynamical descriptions. Instead, our emphasis lies entirely on the thermodynamic characterisation of transport processes. While the formal theoretical frameworks used to describe classical and quantum systems may differ, because of the universal validity of thermodynamic laws, their applicability is independent of whether the underlying system is classical or quantum in nature [4, 10]. Although our discussion is primarily framed in the context of quantum transport, the thermodynamic insights developed throughout this review are equally applicable to classical transport processes. In this sense, the perspective adopted here provides a unified and overarching thermodynamic understanding of coupled transport phenomena.

The primary motivation for studying coupled transport lies in understanding how transport processes are constrained and governed by a clear thermodynamic interpretation. Any transport process is inherently a non-equilibrium phenomenon, involving a departure from an initial equilibrium state, followed by an out-of-equilibrium dynamics and the eventual settlement towards a final equilibrium configuration. The thermodynamic nature of such non-equilibrium processes is encapsulated within a central quantity: the entropy production rate [2, 7, 10]. This quantity serves as the touchstone

---

\* shuvadipg21@iitk.ac.in

† arnab@iitk.ac.in

of non-equilibrium thermodynamics and determines the thermodynamic permissibility of physical processes. A process is thermodynamically allowed *iff* its entropy production rate is non-negative; violation of this condition would contradict the second law of thermodynamics. As a result, non-negative entropy production rate imposes fundamental bounds and limitations on transport properties, deciding both its directionality and efficiency. While transport phenomena can, in principle, be analysed across the full non-equilibrium domain, our interest in this review is restricted to the near-equilibrium regime, where the analytical characterization of the entropy production rate is feasible. Thus, beyond near-equilibrium, thermodynamic analysis becomes fairly intricate and lies outside the scope of this review.

Now, any transport process involves a flux or current. From basic thermodynamics, it is clear that a nonzero flux cannot arise spontaneously; rather, it must be driven by a thermodynamic force. A non-zero force can perturb the system away from equilibrium, thereby inducing a flow of current, and then the system subsequently relaxes toward a new equilibrium state. Forces and fluxes, therefore, constitute the basic building blocks of the theory of thermodynamic transport. In the regime of near-equilibrium, these quantities are linked through the entropy production rate and can be written as the sum of the products of the thermodynamic forces and their conjugate fluxes [1, 2, 7, 11–14]. This formulation provides a transparent and self-consistent framework by which the magnitude, direction, and mutual influence of different currents can be systematically analysed.

A transport process involving a single force-flux pair is conceptually the simplest; also, its near-equilibrium behaviour is comparatively easy to analyse and largely predictable. To access richer and more complex thermodynamic behaviour, it is important to consider situations involving multiple force-flux pairs. This naturally leads to the study of coupled transport with at least two distinct transport processes interlinked with each other. Although in principle the analysis could be extended to systems involving a larger number of coupled force-flux pairs, such frameworks rapidly become untractable and conceptually opaque. Coupled transport, involving exactly two force-flux pairs, thus represents an optimal compromise: it remains rather simple to permit systematic analysis, yet considerably rich to exhibit a wide variety of nontrivial and physically interesting phenomena. Indeed, it underlies the operational principles of several well-known thermodynamic effects [15–23], including Seebeck [1, 2, 18, 24–30] and Peltier effects [1, 2, 26, 30–33], as well as thermoelectric heat engines [18, 20, 34–36] and refrigerators [19, 37–41]. Therefore, a proper thermodynamic understanding of these phenomena becomes an integral part of the theory of coupled transport. In this review, our aim is to elucidate these connections in detail. Beyond conventional thermodynamic cross-effects, we will also explore more subtle and counter-intuitive transport phenomena, such as inverse currents [42, 43].

The remainder of this article is organised as follows. In Section II, we introduce the simplest possible case, namely a single transport process. We then proceed to the central theme of this review — coupled transport. In Section III, we construct a general theoretical framework for investigating quantum coupled transport, including detailed discussions of the system, the environment, and their mutual interactions. We begin our analysis of coupled transport with a single quantum dot (SQD) in a two-terminal configuration. The dynamical evolution and steady-state currents of this model are derived in Section IV. In Section V, we derive a general expression for the entropy production rate, which constitutes the basic framework for the thermodynamic theory presented throughout the review. In Section VI, we identify the relevant force-flux pairs for the SQD model. We then move on to a detailed analysis of coupled transport in the minimal SQD setup. This analysis is carried out case by case in Section VII. In Section VIII, we clarify the subtle but important distinction between conventional thermodynamic cross-effects and the phenomenon of ICC. The discussion is then extended to a more general framework in Section IX, where we analyse coupled transport in a three-terminal coupled QD (CQD) model, which naturally captures the thermodynamics of thermoelectric devices. In Section X, we specifically focus on inverse currents in coupled (ICC) transport, highlighting their physical origin and thermodynamic implications as one of the most counterintuitive outcomes of transport processes. Finally, we conclude the review in Section XI with a summary and outlook.

## II. THERMODYNAMICS OF TRANSPORT PROCESS

We start with a general framework of transport phenomena that is equally applicable to macroscopic and microscopic systems. The permissibility of any physical process is strictly governed by the second law of thermodynamics, which dictates that the entropy production rate ( $\dot{\Sigma}$ ) must be positive for a spontaneous process, while a zero entropy production rate corresponds to a state of thermal equilibrium [1, 2]. For transport phenomena, in the near-equilibrium condition, the entropy production rate can be expressed in terms of the force-flux pairs present in the system as

$$\dot{\Sigma} = \sum_i J_i \mathcal{F}_i \quad (1)$$

where  $J_i$  denotes the  $i$ -th thermodynamic flux and  $\mathcal{F}_i$  is its corresponding conjugate force, interlinked through a cause-and-effect relationship. When a single thermodynamic force is applied, it induces a response in the system in the form of a flux. The resulting flux aligns along the direction of the applied force, which arises from gradients such as temperature or chemical potential. For example, an energy force such as a temperature gradient drives an

energy current in the form of heat flow; thus, the temperature gradient acts as the conjugate force associated with heat transport.

### A. Single Transport Process

If a single force–flux pair is present, the process is termed a single transport, for which thermodynamic analysis is relatively straightforward. In such a process, the entropy production rate reduces to  $\dot{\Sigma} = J\mathcal{F}$ , and implies that the flux should be aligned in the same direction as the conjugate force, otherwise the entropy production rate would be negative. This can be illustrated using an example of a classical heat transfer between two bodies, say  $a$  and  $b$ . Although the sign of currents is a matter of convention, clearly defining it is beneficial to avoid ambiguity in subsequent sections. Let us define any force or flux aligned from  $a$  to  $b$  as positive, while the opposite corresponds to a negative sign. Hence, the energy force is defined as  $\mathcal{F}_a = T_a - T_b$  is positive, indicating that  $a$  is the hotter body, and the entropy production rate is  $\dot{\Sigma} = J_a\mathcal{F}_a > 0$ . This implies that the heat current  $J_a$  must be positive, with the flow of heat from the hotter body  $a$  to the cooler body  $b$ , in complete accordance with the second law of thermodynamics.

The paradigmatic example considered above is the transport of heat (energy), where an energy flux in the form of a heat current arises because of a temperature difference or, more precisely, in the form of an inverse-temperature gradient or thermodynamic force [7, 44]. Another common example is particle or mass transport, where a particle current is generated by a difference in the chemical potential between two regions. This mechanism underlies diffusion processes in which particles migrate from regions of higher chemical potential to lower chemical potential [7, 45]. Similarly, charge transport along a wire represents a single transport process in which an electric current is driven by a voltage difference (electric potential) [46, 47], as observed in electrical conduction through metallic or semiconducting materials [47–49]. Single transport behaviour also arises in spin transport, where a spin current flows in response to a spin bias or a difference in spin chemical potential (for, e.g.  $\Delta\mu_S = \mu_\uparrow - \mu_\downarrow$ ) [50]. Such processes are particularly relevant in magnetic and spintronic systems, where spin degrees of freedom are manipulated independently of charge. In momentum transport, commonly encountered in fluid dynamics, the flux corresponds to momentum flow (expressed through the stress tensor), while the conjugate force is a velocity gradient; this mechanism gives rise to viscous flow in fluids [51]. Unlike in the case of energy or heat transport, where a gradient is directly related to the corresponding thermodynamic force, this equivalence, however, does not hold for all types of transport. This is because the gradient of a physical quantity and the associated thermodynamic force need not always be identical. For instance, in particle trans-

port, the corresponding thermodynamic force is not simply given by the chemical potential difference itself and may instead depend on the respective temperatures as well. Therefore, to ensure thermodynamic consistency and correctness, it is essential to identify the appropriate thermodynamic force. To identify the precise form of the conjugate forces, a detailed analysis of the entropy production rate is required, since current alone cannot determine the actual form of the thermodynamic forces. This will be carried out in the subsequent sections. Moreover, in the linear-response regime, a single transport process takes a simple form in terms of *Onsager kinetic coefficient* [2, 11, 13, 14]. If there is only one force–flux pair present, the flux is influenced by its only conjugate force, and it is characterised by the *direct Onsager coefficient* ( $L$ ), via the relation  $J = L\mathcal{F}$ . Thus, the entropy production rate can be written as  $\dot{\Sigma} = L\mathcal{F}^2 \geq 0$ , which readily implies that  $L$  must be positive.

While the non-negativity of the entropy production rate is universal and remains valid in near equilibrium as well as very far away from equilibrium, the above discussion is primarily valid in the near equilibrium regime, where the entropy production rate is the product of the thermodynamic force and its corresponding flux. The form of the entropy production rate defined in Eq. (1), is not applicable for the far-from-equilibrium condition [2]. There, a current can flow against its conjugate force in a single transport process, yet it is not forbidden by the laws of thermodynamics. Such an intriguing transport phenomenon is the concept of absolute negative mobility (ANM) [52–56], in which the response of the system, i.e., the generated current, operates counter to the driving force. However, ANM cannot exist around a thermal equilibrium, as it would create a perpetual mobile of the second kind, capable of performing work with just a single heat bath. Although ANM was initially considered as a consequence of quantum effects [57, 58], recent studies have explored ANM in various non-equilibrium classical systems, such as tracer dynamics in steady laminar flows [59], self-propulsion [60], particle separation [61, 62], as well as various interacting Brownian motions [52, 62–66]. Furthermore, there has also been experimental evidence to support ANM in the presence of a single force [55, 58, 67]. Thus, single transport processes can exhibit interesting thermodynamic behaviour beyond the near-equilibrium regime, but their detailed analysis lies beyond the scope of this review.

However, if we go beyond single transport and consider coupled transport, exciting thermodynamic phenomena can occur even within the near-equilibrium situation. The interplay between multiple force–flux pairs enables us to offer a variety of thermodynamic effects. The subsequent sections will focus on coupled transport, which constitutes the main body of this perspective article.

## B. Coupled Transport Process

As the name suggests, coupled transport refers to a physical situation where two transport processes coexist and are coupled to each other, with pairs of thermodynamic forces and fluxes. Therefore, to investigate coupled transport, one must consider two distinct types of flow — such as energy and particles, or spin and mass — and construct a model in which these transport processes are simultaneously present and are intrinsically coupled. Here, without loss of generality, we consider energy and particle currents. Following Eq. (1), The general form of the entropy production rate for such a setup takes the simple form:

$$\dot{\Sigma} = J_E \mathcal{F}_E + J_N \mathcal{F}_N, \quad (2)$$

where  $J_E(J_N)$  is the energy (particle) current, conjugate to the energy (particle) force,  $\mathcal{F}_E(\mathcal{F}_N)$ . It is immediately clear that both currents cannot flow simultaneously against their respective conjugate forces. Such a configuration would render the entropy production rate negative, as indicated by Eq. (1), thereby violating the second law of thermodynamics.

However, it is important to emphasise that the mere coexistence of two different transport processes does not necessarily imply coupled transport. If the transport processes are independent, each current is driven solely by its own conjugate force, resulting in a strictly positive rate of entropy production. In such a scenario, no nontrivial thermodynamic behaviour emerges, as the system merely exhibits two independent *single-transport* processes rather than genuine coupled transport. True coupled transport occurs only when each flux responds not only to its conjugate force but also to a non-conjugate force associated with other transport channels. Therefore, we must construct a model in which two transport processes coexist in an integrated manner. Within the linear-response regime, this mutual interdependence can be expressed through Onsager coefficients. For energy and particle currents, they can be written as

$$\begin{aligned} J_E &= L_{EE} \mathcal{F}_E + L_{EN} \mathcal{F}_N, \\ J_N &= L_{NE} \mathcal{F}_E + L_{NN} \mathcal{F}_N, \end{aligned} \quad (3)$$

where,  $L_{EE}$  and  $L_{NN}$  represent the “*direct Onsager coefficients*”, while  $L_{EE}$  and  $L_{NN}$  refer to the “*cross Onsager coefficients*”, fulfilling “*Onsager Reciprocity*” condition  $L_{EE} = L_{NN}$  [13, 14]. While  $L_{EE}$  and  $L_{NN}$  are necessarily positive, the cross coefficients may assume negative values, and it is precisely this property that gives rise to a variety of nontrivial and intriguing transport phenomena. In the case of two independent “*single-transport*” processes, the Onsager cross coefficients vanish, indicating that each flux is unaffected by non-conjugate thermodynamic forces. The presence of nonzero off-diagonal Onsager coefficients signifies genuine coupled transport, where each current responds to both its conjugate and non-conjugate forces. Our next objective is therefore to

identify a suitable model where genuine *quantum coupled transport* (QCT) can be observed.

## III. THE MODEL FOR QUANTUM COUPLED TRANSPORT

The subject of quantum transport has attracted significant attention in recent years because of its rich thermodynamic features and its experimental realizability [18, 20, 28, 49, 68–73]. The theory of quantum transport can be described within the framework of open quantum systems [74–83], where a small quantum system interacts with one or more external reservoirs [Fig. 1]. This general framework consists of three basic constituents: the system, the environment or reservoir, and the interaction between them. Over the years, a variety of standard system–bath models have been proposed in the literature to investigate a wide range of physical processes within this paradigm. Typically, the system is modelled using elementary building blocks such as two-level systems (TLSs) or simple harmonic oscillators, while the reservoirs are composed of bosonic or fermionic degrees of freedom, obeying Bose–Einstein (BE) or Fermi–Dirac (FD) statistics, respectively.

In the present work, our primary focus is on the quantum dot–fermionic reservoir model, which provides a natural platform for studying coupled charge and heat transport. In this setup, quantum dots (QDs)—effectively modelled as TLSs—form the central system, whereas the leads act as fermionic reservoirs composed of electrons. This framework supports both particle (charge) and energy (heat) currents, making it particularly suitable for investigating thermoelectric effects [15–20, 22, 23, 84–87], Maxwell’s demon–type feedback mechanisms [88–91], and transport phenomena relevant to quantum information processing [88, 92, 93]. Consequently, the QD–fermionic reservoir model serves as an ideal candidate to analyse the thermodynamics of coupled transport in nanoscale systems.

Alongside this model, several other well-established theoretical frameworks offer complementary insights into quantum transport phenomena. In particular, the spin–boson [74, 94–99] and Caldeira–Leggett model [100–102] provide canonical descriptions of thermal energy transport and constitute the theoretical foundation for quantum thermal devices such as heat engines [103–105], refrigerators [103, 106–110], rectifiers [83, 111–119], and thermal transistors [80, 120–124]. In these models, the reservoirs are composed of bosonic excitations—such as photons, phonons, or magnons—that act as heat carriers, while the system elements, represented by qubits, harmonic oscillators, or interacting spins, govern the energy exchange dynamics. Furthermore, the Landauer–Büttiker formalism [125] is widely used to describe quantum ballistic transport, in which bosonic or fermionic particles can carry coherent current flow. Together, these models form the theoretical basis for under-

standing nonequilibrium transport in quantum systems.

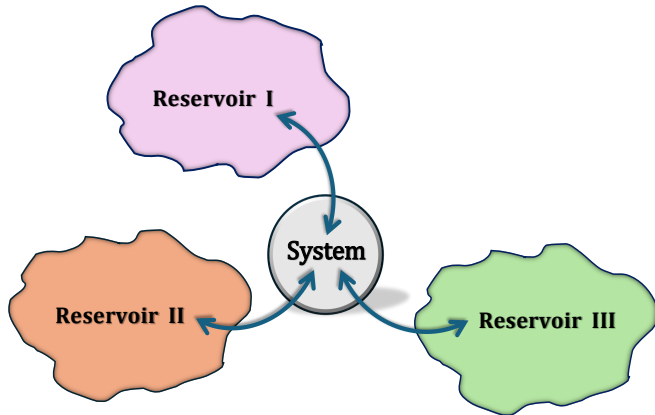


FIG. 1. A small quantum system interacts with multiple reservoirs

### A. System

The key element of our system is the QD. Considering a QD as the building block, one can, however, build more complex systems, like a Double-QD (DQD) [72, 126, 127], Coupled-QD (CQD) [18, 43, 82, 83, 121], Series-coupled QDs (SCQD) [128–131], etc. Now, a single QD can be characterised as a TLS by restricting the occupancy of the QD to either zero or one, where the ground state  $|g\rangle$  implies an empty QD and the only excited state  $|e\rangle$  consists of one particle in the dot. Therefore,  $|g\rangle$  and  $|e\rangle$  can be rewritten in terms of the number states, as  $|0\rangle$  and  $|1\rangle$ , respectively. The system Hamiltonian for a single QD can be defined as

$$H_s = \varepsilon \mathcal{N} = \varepsilon d^\dagger d, \quad (4)$$

where  $\varepsilon$  is the single particle energy level of the QD and  $\mathcal{N} = d^\dagger d$  signifies the number operator of the system, where  $d^\dagger$  ( $d$ ) implies the creation (annihilation) operator of the QD, obeying the anti-commutation relation  $\{d, d^\dagger\} = 1$ . From Eq. (4), the energies of the eigenstates  $|0\rangle$  and  $|1\rangle$  can be evaluated as 0 and  $\varepsilon$ , respectively. In a similar way, one can construct Hamiltonians for DQD, CQD, SCQD systems as well. It is worth pointing out that at this point, we are disregarding the spin of the particle to avoid additional complications.

### B. Environment

For our system-bath model of interest, one or more of the fermionic reservoirs [132–134] are considered as the environment. These baths are essentially filled with fermionic particles (e.g., electrons) that follow FD statistics and are characterised by two parameters: temperature and chemical potential. The Hamiltonian for an

arbitrary bath, labelled as  $\lambda$ , can be identified as

$$H_B^\lambda = \sum_k (\epsilon_k^\lambda - \mu_\lambda) c_{\lambda k}^\dagger c_{\lambda k}, \quad (5)$$

where  $\epsilon_k^\lambda$  is the energy of the non-interacting fermions for the reservoir  $\lambda$ ,  $k$  is the continuous wavenumber,  $\mu_\lambda$  is the chemical potential and  $c_\lambda^\dagger$  ( $c_\lambda$ ) represents the creation (annihilation) operator of the bath [82, 83]. As the baths are also fermionic in nature, bath creation-annihilation operators follow the anti-commutation relation analogous to system operators. If there is more than one bath, the total bath-Hamiltonian can be simply written as  $H_B = \sum_\lambda H_B^\lambda$ .

### C. System-Bath Interaction

The QD system is ‘truly’ open to the baths, allowing both energy and particle exchange between them. The interaction is implemented through tunnelling of the particle. Because this particle tunnelling is associated with an energy flow, it generates both particle and energy currents. We are assuming that the system-bath interaction is weak enough to be within the Born-Markov approximation. This in turn ensures sequential tunnelling, which puts a restriction on simultaneous tunnelling of more than one particle at a time. Finally, imposing the rotating wave approximation, the tunnelling Hamiltonian between any  $\alpha$ -th QD, and a  $\lambda$ -th bath can be written as [82, 135]

$$H_T^{\alpha\lambda} = \hbar \sum_k [t_k^{\alpha\lambda} c_{\lambda k}^\dagger d_\alpha + t_k^{\alpha\lambda*} d_\alpha^\dagger c_{\lambda k}], \quad (6)$$

where  $t_k^{\alpha\lambda}$  represents the tunnelling amplitude.

Now, let us begin with the conceptually simple QD-fermionic reservoir model, consisting of a single QD simultaneously tunnel-coupled to two reservoirs, thereby permitting both energy and particle exchange. We then investigate whether this setup provides a suitable framework for studying coupled transport phenomena or not.

## IV. DYNAMICS AND STEADY-STATE CURRENT OF A SINGLE QD SETUP

The minimal model we consider is a two-terminal setup in which a single QD is tunnel-coupled to two fermionic reservoirs [136], denoted by  $l$  (left) and  $r$  (right), as depicted in Fig. 2(a). The system-bath coupling is assumed to be sufficiently weak to justify a Markovian description of the dynamics. Moreover, due to the restriction of the QD occupancy to either zero or one, transport occurs via sequential tunnelling processes only. Since the system consists of a single QD, the corresponding system Hamiltonian is specified by Eq. (4), with two eigenstates,  $|\mathbb{A}\rangle = |0\rangle$  and  $|\mathbb{B}\rangle = |1\rangle$ , with energies 0 and  $\varepsilon$ , respectively [Fig. 2(b)]. Consequently, the dynamics allow for

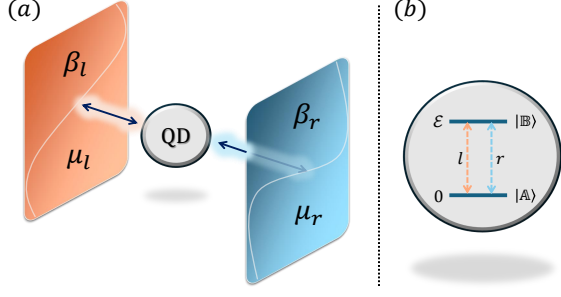


FIG. 2. (a) Two-terminal single QD model for coupled transport (b) Two transitions are induced by the reservoirs.

only a single excitation process  $|\mathbb{A}\rangle \rightarrow |\mathbb{B}\rangle$  that occurs through particle exchange from bath to dot and the corresponding de-excitation process  $|\mathbb{B}\rangle \rightarrow |\mathbb{A}\rangle$ , i.e., particle hopping from dot to lead, forming a closed transition cycle  $|\mathbb{A}\rangle \rightarrow |\mathbb{B}\rangle \rightarrow |\mathbb{A}\rangle$ . Because the QD is simultaneously coupled to both reservoirs, each of these transitions can be mediated by either lead, allowing both energy and particle exchange [Fig. 2(b)]. Since particle tunnelling between a lead and the QD is accompanied by an exchange of energy, the energy transfer is implicitly linked to particle transfer within this model. As a result, the model described above is suitable for investigating coupled transport between energy and particles. It is worth emphasising that the simultaneous coupling of the QD to multiple leads is not a requirement for energy transport, however it is essential to enable net particle transport, a distinction that becomes apparent in the DQD setup [See Sec. IX], where the particle current arises due to inter-dot particle hopping [126].

Because of the simplicity of this model, its qualitative dynamics can be easily understood. If both excitation and de-excitation are mediated by the same reservoir, there is no net particle transfer, and both the particle and energy currents vanish. To generate nonzero particle and energy currents through the QD, the transition cycle must involve different reservoirs for excitation and de-excitation. This condition establishes the basis for studying genuine coupled transport.

To proceed with a quantitative analysis, we must solve the dynamics of the system. Since our system–bath model follows Markovian dynamics, we employ the Lindblad master equation (LME) formalism [74]. Under Born, Markov, and secular (BMS) approximations [74, 126], the LME takes the form [See Appendix- A]

$$\frac{d}{dt}\rho_s(t) = \sum_{\lambda} \mathcal{L}_{\lambda}[\rho_s(t)] \quad ; \quad \lambda = l, r. \quad (7)$$

Here, the reduced state of the composite system is represented by the density matrix  $\rho_s(t) = \text{Tr}_{\text{B}}\{\rho_{\text{tot}}(t)\}$ , where  $\rho_{\text{tot}}(t)$  is the full density matrix of the system and bath combined, where the form of the Lindblad super-operator  $\mathcal{L}_{\lambda}[\rho_s(t)]$  is given in the Appendix- A. The general expressions for the steady state energy and particle currents for

the  $\lambda$ -th reservoir are given by [See Appendix- B]

$$J_{\text{E}}^{\lambda} = \text{Tr}_{\text{s}}[\mathcal{L}_{\lambda}[\rho_{ss}]H_{\text{s}}]; \quad J_{\text{N}}^{\lambda} = \text{Tr}_{\text{s}}[\mathcal{L}_{\lambda}[\rho_{ss}]\mathcal{N}], \quad (8)$$

where  $\rho_{ss}$  signifies the steady-state density matrix. The expression for the steady-state heat current thus simplifies to

$$J_{\text{Q}}^{\lambda} = J_{\text{E}}^{\lambda} - \mu_{\lambda}J_{\text{N}}^{\lambda} = \text{Tr}_{\text{s}}[\mathcal{L}_{\lambda}[\rho_{ss}]H_{\text{s}}] - \mu_{\lambda} \text{Tr}_{\text{s}}[\mathcal{L}_{\lambda}[\rho_{ss}]\mathcal{N}]. \quad (9)$$

With the explicit form of the Lindbladians,  $\mathcal{L}_{\lambda}[\rho_{ss}]$ , defined in Appendix-A [cf. (A6)], the general expressions for the energy and particle currents lead to

$$\begin{aligned} J_{\text{E}}^{\lambda} &= \sum_{\{\omega_{ij}\}} \omega_{ij}\Gamma_{ij}^{\lambda+} = \sum_{\{\omega_{ji}\}} \omega_{ji}\Gamma_{ji}^{\lambda-}; \\ J_{\text{N}}^{\lambda} &= \sum_{\{\omega_{ij}\}} \Gamma_{ij}^{\lambda+} = \sum_{\{\omega_{ji}\}} \Gamma_{ji}^{\lambda-}, \end{aligned} \quad (10)$$

where the net transition rate from level  $|\mathbb{i}\rangle$  to  $|\mathbb{j}\rangle$  driven by tunnelling of the particle from (to) the reservoir  $\lambda$  to (from) the QD is represented by  $\Gamma_{ij}^{\lambda\pm}$ , which is given by

$$\Gamma_{ij}^{\lambda\pm} \equiv \Gamma_{i \rightarrow j}^{\lambda\pm} = \gamma_{\lambda} f_{\lambda}^{\pm}(\omega_{ij})\rho_i - \gamma_{\lambda} f_{\lambda}^{\mp}(\omega_{ji})\rho_j = \Gamma_{i \rightarrow j}^{\lambda\pm} - \Gamma_{j \rightarrow i}^{\lambda\mp}. \quad (11)$$

The first term denotes the transition from the eigenstate  $|\mathbb{i}\rangle$  to  $|\mathbb{j}\rangle$  driven by particle excitation (or de-excitation), while the second term represents the reverse transition  $|\mathbb{j}\rangle \rightarrow |\mathbb{i}\rangle$ , driven by particle de-excitation (or excitation) w.r.t the system. From Eq. (11), it follows  $\Gamma_{ij}^{\lambda+} = -\Gamma_{ji}^{\lambda-}$ , where,  $f_{\lambda}^{\pm}(\omega_{ij})$  denotes the Fermi–Dirac distribution (FDF) function. It is associated with the transition  $|\mathbb{i}\rangle \rightarrow |\mathbb{j}\rangle$  induced by the reservoir  $\lambda$ , with the transition energy  $\omega_{ij}$ . Throughout this article [18, 43, 137], the notation “ $\pm$ ” is used where the “ $+$ ” sign corresponds to particle excitation (i.e., tunnelling into the system), whereas the “ $-$ ” sign refers to particle de-excitation (i.e., tunnelling out of the system). If the transition  $|\mathbb{i}\rangle \rightarrow |\mathbb{j}\rangle$  is governed by particle excitation w.r.t the system, the reverse transition corresponds to particle tunnelling from the system into the lead. This observation allows us to establish a relation between the FDFs for forward and reverse processes [83, 138]:

For the single-QD system connected to two terminals, the dot possesses only two eigenstates,  $|\mathbb{A}\rangle$  and  $|\mathbb{B}\rangle$ , and is tunnel-coupled to the left  $l$  and right  $r$  leads. Under these conditions, the general form of the energy current [cf. (10)] simplifies to

$$J_{\text{E}}^l = \omega_{\text{AB}}\Gamma_{\text{AB}}^{l+} = \varepsilon\Gamma_{\text{AB}}^{l+} \quad ; \quad J_{\text{E}}^r = \omega_{\text{AB}}\Gamma_{\text{AB}}^{r+} = \varepsilon\Gamma_{\text{AB}}^{r+}. \quad (12)$$

The non-zero energy and particle transport between the reservoirs occurs exclusively through two transition pathways — excitation by lead  $l$  and de-excitation by lead  $r$ , or vice-versa. Thus, in the steady state, the associated transition rates obey

$$\Gamma_{\text{AB}}^{l+} = \Gamma_{\text{BA}}^{r-} \equiv \Gamma_{+} \quad ; \quad \Gamma_{\text{AB}}^{r+} = \Gamma_{\text{BA}}^{l-} \equiv \Gamma_{-}, \quad (13)$$

implying  $\Gamma_+ = -\Gamma_-$ . Finally, we obtain the energy current as

$$J_E^l = -J_E^r = \varepsilon\Gamma_+ \quad (14)$$

Similarly, the particle current defined in Eq. (10), yields

$$J_N^l = -J_N^r = \Gamma_+ \quad (15)$$

From Eqs. (14) and (15), it is evident that the energy and particle currents are linearly dependent via a relation  $J_E^{l(r)} = \varepsilon J_N^{l(r)}$ . Having derived analytical expressions for the currents in this minimal QD-reservoir model, we next determine the corresponding thermodynamic forces by analysing the entropy production rate. We first carry out this analysis in a general open quantum system framework with multiple reservoirs and then specialise the result to the present two-terminal single-QD model.

## V. DERIVING ENTROPY PRODUCTION RATE FOR GENERAL QD-FERMIONIC RESERVOIR MODEL

In this section, we derive the fundamental thermodynamic relations for the entropy production rate. We consider a general setup, where a QD system (it may be a CQD or DQD as well) is coupled with multiple baths through particle and energy exchange. Starting with the definition of the entropy change of the system, one can write down the following relation [139]

$$\Delta\mathcal{S}_s(t) = \Sigma(t) + \Phi(t), \quad (16)$$

where, the *entropy production* term  $\Sigma(t)$  signifies the irreversible contribution of the system entropy change and  $\Phi(t)$  term refers to the *entropy flux*. At close to equilibrium, we equate the von Neumann entropy (times  $k_B$ ) with thermodynamic entropy as

$$\mathcal{S}_s(t) = -k_B \text{Tr}_s[\rho_s(t) \ln \rho_s(t)]. \quad (17)$$

From Eq. (16), we can evaluate

$$\begin{aligned} \Delta\mathcal{S}_s(t) &= \mathcal{S}_s(t) - \mathcal{S}_s(0) \\ &= -k_B \text{Tr}[\rho_{\text{tot}}(t) \ln \rho_s(t)] + k_B \text{Tr}[\rho_{\text{tot}}(0) \ln \rho_s(0)] \end{aligned} \quad (18)$$

Substituting the initial equilibrium state of the compound system as

$$\rho_{\text{tot}}(0) = \rho_s(0) \prod_{\lambda} \rho_{\lambda}^{\text{eq}}, \quad (19)$$

in the absence of any entanglement or correlation, in Eq. (18), the final expression of  $\Delta\mathcal{S}_s(t)$  can be evaluated as

$$\begin{aligned} \Delta\mathcal{S}_s(t) &= -k_B \text{Tr} \left[ \rho_{\text{tot}}(t) \ln \left\{ \rho_s(t) \prod_{\lambda} \rho_{\lambda}^{\text{eq}} \right\} \right] \\ &\quad + k_B \text{Tr}[\rho_{\text{tot}}(t) \ln \rho_{\text{tot}}(t)] \\ &\quad + k_B \sum_{\lambda} \text{Tr}_{\lambda} [\{\rho_{\lambda}(t) - \rho_{\lambda}^{\text{eq}}\} \ln \rho_{\lambda}^{\text{eq}}], \end{aligned} \quad (20)$$

In deriving the above equation, we have used the relation  $\rho_{\text{tot}}(t) = \mathcal{U}\rho_{\text{tot}}(0)\mathcal{U}^{\dagger}$ , i.e., states  $\rho_{\text{tot}}(t)$  and  $\rho_{\text{tot}}(0)$  are unitarily related to each other.

The last term in Eq. (20) can be identified as the *entropy flow* ( $\Phi$ ), representing the reversible contribution to the system entropy change due to heat exchanges. A comparison of the above equation with Eq. (16), help us to define the *entropy production* and the *entropy flow* as,

$$\begin{aligned} \Sigma(t) &= \text{Tr}[\rho_{\text{tot}}(t) \ln \{\rho_{\text{tot}}(t)\}] \\ &\quad - \text{Tr} \left[ \rho_{\text{tot}}(t) \ln \left\{ \rho_s(t) \prod_{\lambda} \rho_{\lambda}^{\text{eq}} \right\} \right], \quad (21) \\ \Phi(t) &= \sum_{\lambda} \text{Tr}_{\lambda} [\{\rho_{\lambda}(t) - \rho_{\lambda}^{\text{eq}}\} \ln \rho_{\lambda}^{\text{eq}}], \end{aligned}$$

where,  $\rho_{\lambda}^{\text{eq}}$  and  $\rho_{\lambda}(t)$  represent the density operators of the  $\lambda$ 'th reservoir under equilibrium and *near equilibrium* conditions, respectively. Moreover,  $\rho_{\lambda}^{\text{eq}}$  can be written as

$$\rho_{\lambda}^{\text{eq}} = \frac{e^{-\beta_{\lambda} H_B^{\lambda}}}{\mathcal{Z}_{\lambda}(\beta_{\lambda})}, \quad (22)$$

where  $H_B^{\lambda} = \sum_k (\epsilon_k^{\lambda} - \mu_{\lambda}) c_{\lambda k}^{\dagger} c_{\lambda k}$  and  $\mathcal{Z}_{\lambda}(\beta_{\lambda}) = \text{Tr} [e^{-\beta_{\lambda} H_B^{\lambda}}]$  is the the grand canonical partition function for the  $\lambda$ 'th reservoir. As a result,  $\Phi(t)$  is identified as the heat exchange with the reservoir

$$\Phi(t) = k_B \sum_{\lambda} \beta_{\lambda} \Delta Q_{\lambda}(t), \quad (23)$$

between the final and initial time:  $\Delta Q_{\lambda}(t) = \langle H_B^{\lambda} \rangle_0 - \langle H_B^{\lambda} \rangle_t$ , with  $\langle H_B^{\lambda} \rangle_t = \text{Tr}_{\lambda} [\rho_{\lambda}(t) H_B^{\lambda}]$ . Thus, we can rewrite Eq. (16) as

$$\Delta\mathcal{S}_s(t) = \Sigma(t) + k_B \sum_{\lambda} \beta_{\lambda} \Delta Q_{\lambda}(t), \quad (24)$$

where we replace the second term by Eq. (23). The entropy production rate can then be deduced from the above equation as follows,

$$\dot{\Sigma}(t) = \frac{d}{dt} \{\Delta\mathcal{S}_s(t)\} - k_B \sum_{\lambda} \beta_{\lambda} J_Q^{\lambda}(t). \quad (25)$$

where, we define  $J_Q^{\lambda}(t) = \frac{d}{dt} \{\Delta Q_{\lambda}(t)\}$ . At the *steady state*,  $\dot{\Sigma}$  becomes minimum [126, 139, 140] and  $\frac{d}{dt} \{\Delta\mathcal{S}_s(t)\} = 0$ . Therefore, Eq. (25) yields

$$\dot{\Sigma} = -k_B \sum_{\lambda} \beta_{\lambda} J_Q^{\lambda}. \quad (26)$$

Again, if steady-state heat currents are defined in terms of energy and particle currents as  $J_Q^{\lambda} = J_E^{\lambda} - \mu_{\lambda} J_N^{\lambda}$ , the above equation can be expressed as

$$\dot{\Sigma} = -k_B \sum_{\lambda} \beta_{\lambda} J_E^{\lambda} + k_B \sum_{\lambda} \left( \frac{\beta_{\lambda}}{\mu_{\lambda}} \right) J_N^{\lambda}. \quad (27)$$

To analyse the preceding expression, we require explicit analytical forms of the energy and particle currents associated with an arbitrary reservoir  $\lambda$ , namely  $J_E^\lambda$  and  $J_N^\lambda$ . These currents have already been evaluated for our minimal single-QD two-terminal configuration. Examining the resulting entropy production rate allows us to identify the thermodynamic forces corresponding to energy and particle transport in this setup. This, in turn, enables a formulation of coupled transport within the force-flux framework. Accordingly, in the next section, we derive the explicit force-flux pairs for our model and proceed to the central goal of this work: a detailed thermodynamic analysis of coupled transport phenomena.

## VI. IDENTIFYING THE THERMODYNAMIC FORCE-FLUX PAIRS FOR TWO-TERMINAL SINGLE QD SETUP

Based on the general expression of the entropy production rate defined in Eq. (27), we identify the force-flux pairs within two terminal single QD model, as

$$\dot{\Sigma} = -k_B[\beta_l J_E^l + \beta_r J_E^r] + k_B[\beta_l \mu_l J_N^l + \beta_r \mu_r J_N^r]. \quad (28)$$

As there is no external source or sink, the net energy and particle currents are conserved in the steady state, i.e.,  $\sum_\lambda J_E^\lambda = \sum_\lambda J_N^\lambda = 0$ . This leads to four equivalent expressions for the entropy production rate:

$$\dot{\Sigma} = \begin{cases} J_E^l \mathcal{F}_E^l + J_N^l \mathcal{F}_N^l \\ J_E^r \mathcal{F}_E^r + J_N^r \mathcal{F}_N^r \\ J_E^l \mathcal{F}_E^r + J_N^l \mathcal{F}_N^r \\ J_E^r \mathcal{F}_E^l + J_N^r \mathcal{F}_N^l \end{cases} \quad (29)$$

where the thermodynamic forces are defined as:

$$\begin{aligned} \mathcal{F}_E^l &= -\mathcal{F}_E^r = k_B(\beta_r - \beta_l), \\ \mathcal{F}_N^l &= -\mathcal{F}_N^r = k_B(\beta_l \mu_l - \beta_r \mu_r). \end{aligned} \quad (30)$$

Let us again reiterate the convention used for forces and fluxes: When a current ( $J_E^\lambda$ ,  $J_N^\lambda$  or  $J_Q^\lambda$ ) enters the system from reservoir  $\lambda$ , the sign of the current is considered positive, i.e.,  $J^\lambda > 0$ . In the case of the forces, it follows from Eq. (30) that a positive energy force  $\mathcal{F}_E^l > 0$  implies  $\beta_l < \beta_r$ , whereas  $\mathcal{F}_E^r > 0$  implies  $\beta_r < \beta_l$ . Although these two forces describe the same physical situation, they are related by  $\mathcal{F}_E^l = -\mathcal{F}_E^r$ . Therefore, to determine the direction of the forces solely from their signs, one must adopt a form of the entropy production rate that uses consistent labels (either  $l$  or  $r$ ) for both energy and particle fluxes and forces. This leaves us with two equivalent choices:

$$\dot{\Sigma} = J_E^l \mathcal{F}_E^l + J_N^l \mathcal{F}_N^l = J_E^r \mathcal{F}_E^r + J_N^r \mathcal{F}_N^r. \quad (31)$$

Without loss of any generality, we choose  $\dot{\Sigma} = J_E^l \mathcal{F}_E^l + J_N^l \mathcal{F}_N^l$ .

To proceed, we clarify a subtle but important distinction between gradients and thermodynamic forces. Although related, they are *distinct thermodynamic quantities*. For energy transport, the thermodynamic force coincides with the temperature gradient in the linear-response (near-equilibrium) regime with  $\mathcal{F}_E^l = k_B(\beta_r - \beta_l) = \frac{\Delta T}{T_l T_r}$ . In contrast, the particle force  $\mathcal{F}_N^l = k_B(\beta_l \mu_l - \beta_r \mu_r)$  reduces to the chemical potential gradient only when  $T_l = T_r = T$ . For  $\Delta T \neq 0$ , we have  $\mathcal{F}_N^l = \frac{\Delta \mu}{T_l} - \mu_r \mathcal{F}_E^l$ . Thus,  $\mathcal{F}_N^l$  approximates  $\Delta \mu$  only for small  $\Delta T$ . Its sign can even differ from that of  $\Delta \mu$  when  $\frac{\mu_r}{T_r} |\Delta T| > |\Delta \mu|$ . This raises a natural question: why are the chemical potential gradient and the particle force so often used interchangeably [1, 2, 18, 136, 141] in the literature? The reason is practical. In macroscopic and most mesoscopic systems, this condition is rarely met, so the two are used interchangeably. However, on the nanoscale, with  $\mu_r$  and  $\Delta \mu \sim 10-80 \mu\text{eV}$  and  $T_r$  and  $\Delta T \sim 10-100 \text{mK}$ , above inequality can easily be satisfied, which is precisely the regime relevant for the quantum transport models considered here. Thus, interpreting transport in this regime, solely based on  $\Delta \mu$  can be misleading: a particle current may appear to flow against the gradient while actually flowing along its true thermodynamic force. Since entropy production is defined in terms of thermodynamic forces rather than gradients, transport — especially at the nanoscale — must be characterised using the correct thermodynamic forces.

## VII. THERMODYNAMICS OF COUPLED TRANSPORT IN TWO TERMINAL SINGLE QD SETUP

We now explore the thermodynamics of coupled transport in a two-terminal single-QD model, involving one energy and one particle force-flux pair. For a systematic analysis, we examine the behaviour case by case.

### A. Both $\mathcal{F}_E^l$ and $\mathcal{F}_N^l$ are zero

As expected, when both forces are zero, no driving mechanism exists in the system, and consequently both the energy and the particle currents are zero, implying a state of thermal equilibrium, with  $\dot{\Sigma} = 0$ . According to Eq. (30),  $\mathcal{F}_E^l = \mathcal{F}_N^l = 0$  correspond to both leads being in the same temperature and chemical potential. Microscopically, under these conditions, the transition cycle  $|\mathbb{A}\rangle \rightarrow |\mathbb{B}\rangle \rightarrow |\mathbb{A}\rangle$  is equally likely to be initiated by the left or right reservoir. As a result, a cycle in which excitation is governed by the left lead and de-excitation by the right lead is equally likely to its reverse process. So, there is no net particle transfer between the system and either reservoir, and the average particle current vanishes. Consequently, the energy current also vanishes, as the two currents are related through the proportionality factor  $\varepsilon$ . In summary, when both forces are zero, we obtain the

trivial result, marked as the origin in the 2D-diagram in Fig. 3.

### B. Seebeck effect in presence of only energy force

Now, in the presence of the only energy force  $\mathcal{F}_E^l$  (i.e. on the x-axis of Fig. 3), the energy current  $J_E^l$  must be in the same direction to make the entropy production rate non-negative. Hence, without loss of generality, if we consider  $\mathcal{F}_E^l > 0$  by choosing  $\beta_r > \beta_l$  [cf. (30)],  $J_E^l$  must also be positive. This is the expected thermodynamic behaviour under an applied temperature gradient, i.e., heat flow from the left (hot) reservoir to the right (cold) reservoir. However, there is no thermodynamic restriction on the direction of  $J_N^l$ , since  $\mathcal{F}_N^l = 0$  and thus does not contribute to the entropy production rate. Hence,  $J_N^l$  may assume either sign, implying that it can flow from left to right or from right to left. Thus, the model can support a nonzero particle current even in the absence of a particle force. In this case, the particle current is driven by the energy current because of the nonzero energy force, which acts as a non-conjugate driving force for particle transport. This intriguing physical phenomenon is known as a thermodynamic cross effect, wherein a nonzero thermodynamic current is driven by a non-conjugate force, in the absence of its conjugate force.

Within the linear response regime, this situation can be explained via Onsager coefficients [cf. Eq. (3)]. Since  $J_N^l = L_{NE}\mathcal{F}_E^l + L_{NN}\mathcal{F}_N^l$  and  $\mathcal{F}_N^l = 0$ , it reduces to  $J_N^l = L_{NE}\mathcal{F}_E^l$ . As the Onsager cross coefficient can assume positive or negative values, the nonzero particle current is driven by the non-conjugate energy force  $\mathcal{F}_E^l$ , even in the absence of the conjugate particle force  $\mathcal{F}_N^l$ . This situation corresponds to the well-known Seebeck effect, wherein a temperature gradient induces a particle (or charge) current. Depending on the sign of the cross coefficient  $L_{NE}$ , two distinct regimes can be identified [Fig. 3]. For  $L_{NE} > 0$ ,  $J_N^l$  flows along the direction of  $\mathcal{F}_E^l$ . This is the conventional Seebeck effect [1, 2, 18, 24–26, 28, 30, 82]. In contrast, for  $L_{NE} < 0$ , the particle current flows opposite to the applied energy force, a situation that can be identified as the unconventional Seebeck effect. The Seebeck effect provides the fundamental thermodynamic principle underlying a thermoelectric heat engine. In the present two-terminal single-QD model, however, the direction of the particle current  $J_N^l$  is constrained by the relation  $J_E^l = \varepsilon J_N^l$ . Since  $\varepsilon > 0$ , both the energy and particle currents are necessarily positive and aligned in the same direction. Thus, we obtain  $J_N^l > 0$  even when  $\mathcal{F}_N^l = 0$ . The proportionality between the energy and particle currents enforces a positive particle current. The model therefore supports the normal Seebeck effect. A unconventional seebeck effect cannot occur within this model, since the particle and energy currents are constrained to flow in the same direction.

### C. Peltier effect in presence of only particle force

We now consider the case where  $\mathcal{F}_E^l = 0$  but  $\mathcal{F}_N^l$  is nonzero, i.e. on the y-axis of Fig. 3. To analyse this case, we take  $\mathcal{F}_N^l > 0$ , which corresponds to  $\beta_l\mu_l > \beta_r\mu_r$  [cf. Eq. (30)]. As anticipated, the resulting particle current  $J_N^l$  is positive, indicating particle flow from the left to the right reservoir. This follows directly from Eq. (3):  $J_N^l = L_{NN}\mathcal{F}_N^l$ . With  $\mathcal{F}_N^l$ ,  $L_{NN} > 0$ , the  $J_N^l$  shares the sign of its conjugate force,  $\mathcal{F}_N^l$ .

In contrast, the energy current  $J_E^l = L_{EN}\mathcal{F}_N^l$  is governed by the Onsager cross coefficient  $L_{EN}$ , which may be positive or negative [Fig. 3]. Thus, even for  $\mathcal{F}_N^l > 0$ , the energy current  $J_E^l$  can flow in either direction [cf. Eq. (3)]. If  $L_{EN} > 0$ , then  $J_E^l > 0$ , corresponding to energy flow from left to right — the conventional Peltier effect [1, 2, 26, 30–33, 82, 142]. If  $L_{EN} < 0$ , the energy current is driven opposite to the particle force, producing  $J_E^l < 0$  and energy flow from right to left, corresponding to a unconventional Peltier effect.

The Peltier effect constitutes the thermodynamic principle that underlies the operation of a refrigerator. However, in the present two-terminal single-QD model, the currents are constrained by  $J_E^l = \varepsilon J_N^l$ . As a result, the energy and particle currents are necessarily aligned. Therefore, only a positive Peltier effect can occur; a unconventional Peltier effect is excluded by this proportionality constraint. In the following, we consider the regime in which both thermodynamic forces are nonzero and investigate whether this setup can function as a thermodynamic heat engine or a refrigerator, operating on the basis of the Seebeck and Peltier effects.

### D. In the presence of both energy and particle force:

In this discussion, we consider the case where both thermodynamic forces are nonzero, under which the coupled transport phenomena become particularly rich. When both thermodynamic forces are nonzero, the parameter space naturally divides into four quadrants [Fig. 3]. The first and third quadrants are equivalent, with mutually parallel forces. As the overall sign is merely a matter of convention, the first and third quadrants describe the same physical behaviour. Similarly, the second and fourth quadrants are isomorphic in nature, with antiparallel forces, i.e., one force acts against the other. We first restrict our attention primarily to the first quadrant, where both forces are positive, and then discuss the difference with the other quadrants.

1. In the first quadrant, when both  $\mathcal{F}_E^l$  and  $\mathcal{F}_N^l$  are positive. Two allowed configurations can arise under this situation: (a) Both energy and particle currents are positive, which is the most natural and expected thermodynamic response when both driving forces are positive. (b) One of the cur-

rents—either the energy or the particle current—is negative, while the other remains positive. The latter case is highly nontrivial and counterintuitive, as it corresponds to a situation in which a particular flux flows against both applied forces, including its own conjugate force. Nevertheless, this behaviour is fully consistent with thermodynamics, provided  $\dot{\Sigma} \geq 0$ . This result is a direct manifestation of coupled transport and is known as the inverse current in coupled (ICC) transport, a phenomenon that was recently identified in a classical Hamiltonian system by Wang *et. al.* [42]. Later, this phenomenon has also been investigated in quantum transport processes [131, 137]. A general definition of ICC, which remains valid for multi-terminal models as well, can be stated as follows: *when two thermodynamic forces are mutually parallel, one of the induced currents flows against both forces.* Although the sign convention of a current is arbitrary, the defining characteristic of ICC is that *a current must simultaneously oppose both mutually parallel thermodynamic forces.* It is therefore evident that negative cross effects act as a necessary precursor for the emergence of a genuine ICC. Specifically, if a current can flow against its non-conjugate force in the absence of the conjugate force, then there exists the possibility for that current to also flow against its conjugate force when both forces are present. Thus, an *unconventional Seebeck* or *unconventional Peltier effect* inherits the possibility of realising an ICC in the energy or particle current, respectively. Such behaviour may be classified as pseudo-ICC. However, it does not constitute a true or genuine ICC, due to the absence of the conjugate force itself. For this reason, regimes described by pseudo-ICC serve as a necessary prerequisite for the emergence of genuine ICC behaviour. Realising a genuine ICC is considerably more challenging than achieving a pseudo-ICC. Thus, it represents a highly counterintuitive and nontrivial manifestation of coupled transport.

In the present two-terminal single-QD setup, we have already ruled out the possibility of realizing either an unconventional Seebeck or an unconventional Peltier effect. Consequently, this minimal model cannot support an ICC phenomenon. In subsequent discussions, we will construct a model capable of exhibiting the ICC phenomenon. Although achieving ICC is highly nontrivial, the realisation of ICC in the particle current or the energy current naturally corresponds to the operation of an autonomous thermoelectric engine or a refrigerator, respectively. Therefore, it carries profound thermodynamic significance in the study of coupled transport processes.

2. We now consider the fourth quadrant of Fig. 3, where the energy force is positive, acting from the

left reservoir to the right, while the particle force is negative, acting in the opposite direction. As noted earlier, a positive energy force corresponds to  $\beta_r > \beta_l$  [cf. Eq. (30)], while  $\beta_r \mu_r > \beta_l \mu_l$  implies a negative particle force [cf. Eq. (30)]. The thermodynamically favoured response is that each current flows along its conjugate force: the energy current is positive, corresponding to heat flow from the hot left reservoir to the cold right reservoir, and the particle current is negative, indicating transport from right to left. This configuration guarantees a strictly positive entropy production rate and is therefore consistent with the second law. However, alternative current configurations are also allowed, provided that the entropy production remains non-negative. The energy current may remain aligned with its force while driving the particle current in the same direction, so that the particle current flows against its own force. In contrast, the particle current may align with its force and drag the energy current in the same direction, causing the energy current to flow against its conjugate force. These two regimes correspond, respectively, to the operation of a thermoelectric heat engine and a refrigerator. In both cases, the behaviour arises from thermodynamic cross effects, in which a non-conjugate force drives a current against its own conjugate force.

Therefore, in the two-terminal single-QD model, the fourth quadrant allows either engine or refrigeration behaviour. An analogous situation arises in the second quadrant (Fig. 3), where the energy force is negative, and the particle force is positive. In this regime also, two thermodynamically allowed outcomes are possible: both currents may be positive, corresponding to refrigeration, or both may be negative, indicating thermoelectric heat-engine operation.

From the above discussion, we identify two fundamentally distinct outcomes of coupled transport: thermodynamic cross effects and inverse current phenomena. Although closely related, these effects differ in a subtle but crucial way. While physical consequences of cross effects have been extensively studied over several decades [2, 11, 13, 14, 68, 143], with thermoelectric heat engines and refrigerators serving as canonical examples, inverse current phenomena, namely, ICC — remain largely unexplored. In the following sections, we first clarify the distinction between these two phenomena and therefore seek a more versatile model capable of exhibiting richer thermodynamic behaviour, including both pseudo-ICC and genuine ICC.

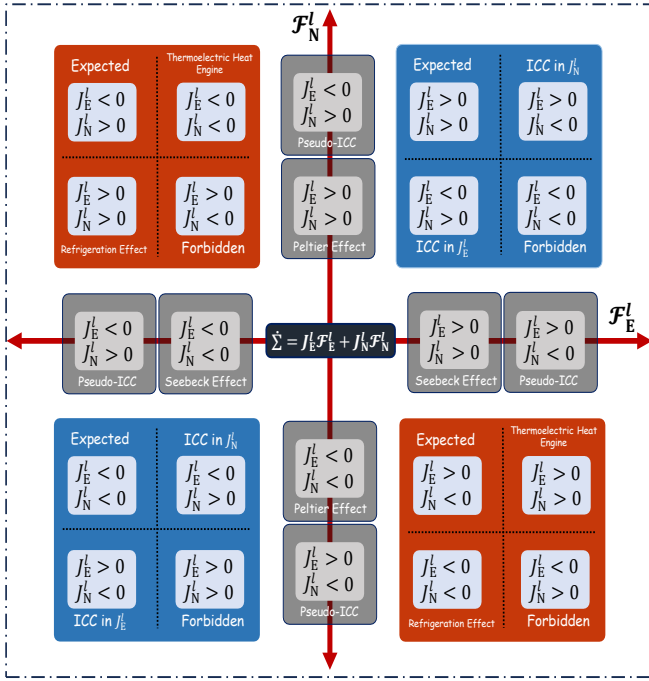


FIG. 3. Pictorial representation of various thermodynamic phenomena governed by the entropy production rate  $\dot{\Sigma} = J_E^l \mathcal{F}_E^l + J_N^l \mathcal{F}_N^l$  i.e., normal cross-effect (red shaded), ICC (blue shaded), pseudo-ICC, Seebeck and Peltier effects that can be obtained.

### VIII. CROSS-EFFECT VS ICC

At first glance, the distinction between ICC and thermodynamic cross effects may appear subtle, since in both cases a current flows against its conjugate force. For example, when a particle current flows against its conjugate particle force, the system functions as a thermoelectric heat engine, whereas when an energy current flows against a temperature gradient, refrigeration occurs. These are the familiar, “traditional” manifestations of thermodynamic cross effects, where an induced current (generated by its non-conjugate force) is driven against its conjugate force. By contrast, the defining feature of ICC is that a current flows against both driving forces — more precisely, against two mutually parallel thermodynamic forces. In this regime, the current is not assisted by any non-conjugate force; instead, it opposes both forces simultaneously. This requirement makes ICC much more counterintuitive and challenging. Although ICC can realise *autonomous* engine or refrigeration behaviour, such devices are fundamentally different from traditional ones: both driving forces oppose a flux, and the system operates autonomously, without any force aiding the current.

### IX. THREE TERMINAL CQD-MODEL FOR COUPLED TRANSPORT

In this section, we focus on a capacitively coupled three-terminal CQD setup [18, 43, 82, 83, 121] rather than a conventional DQD system [72, 126, 127]. While coupled transport in a DQD configuration can arise from weak inter-dot hopping, such systems consist of two nearly independent single-QD Hamiltonians connected by a small tunnelling term. In contrast, strong capacitive coupling in a CQD fundamentally modifies the system’s Hilbert space, rendering it a genuinely composite quantum system whose Hamiltonian is diagonal in the joint eigenbasis of the two QD’s number operators. We further extend this two terminal single-QD model to a three-terminal CQD configuration, where an auxiliary QD is tunnel-coupled to an additional electronic (fermionic) reservoir without directly participating in charge transport between the primary leads. This model resembles to the well-established three-terminal Sánchez–Büttiker model [18], which has been widely studied [20, 22, 88, 92, 93, 138, 144–152] and experimentally realised as a three-terminal energy-harvesting device by Thierschmann et al. [20]. We adopted this framework over DQD because three-terminal CQD devices spatially separate the heat reservoir from the conducting channel, enabling partial decoupling of energy and particle currents and allowing higher thermodynamic efficiencies than conventional two-terminal setups. This makes the CQD platform more versatile for investigating thermoelectric effects and ICC phenomena. In the following, we first discuss thermoelectric effects in three-terminal setup, then briefly review the novel ICC effect in a similar setup.

#### A. Thermoelectric effects in three terminal CQD setup

In this section, we study coupled transport in a three-terminal CQD model. We first discuss the model and then develop its thermodynamic force–flux formulation to analyse coupled energy and particle transport within this setup. In a suitable limit, the setup is reduced to the two-terminal single-QD case, retaining all the corresponding thermoelectric effects.

##### 1. Model

The model consists of two strongly and capacitively coupled QDs, denoted as the upper dot (QD<sub>u</sub>) and the bottom dot (QD<sub>b</sub>), as schematically illustrated in Fig. 4(a). The QDs interact exclusively through long-range Coulomb interaction, suppressing direct particle exchange due to Coulomb blockade, while enabling energy exchange between the dots via a capacitive coupling of strength  $\kappa_c$  [83, 148, 153]. Although the QDs are

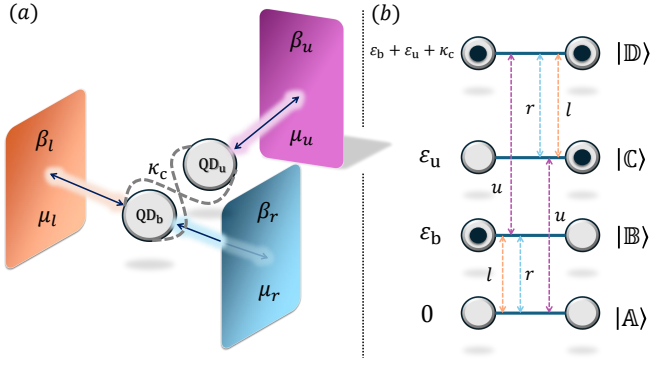


FIG. 4. (a) Schematic of the three-terminal CQD model. (b) Energy level diagram of CQD where transitions are mediated by the baths within the eigen-states of the composite system.

strongly and capacitively coupled, we still assume that the system-reservoir interaction is weak enough so that the Markovian dynamics can be followed for the reduced system dynamics. The QD<sub>b</sub> is simultaneously tunnel-coupled to two fermionic reservoirs, labelled *l* (left) and *r* (right), thereby allowing particle transport between these two leads [18, 83, 134, 154]. In contrast, QD<sub>u</sub> is tunnel-coupled to a single electronic reservoir, allowing particle and energy exchange between the dot and the reservoir. If we focus on the lower subsystem, namely QD<sub>b</sub>, which is tunnel-coupled to both reservoirs *l* and *r*, it effectively reproduces the two-terminal single-QD model discussed in Sec. IV. For spinless electrons,  $\kappa_c$  is necessarily positive. Therefore, the Hamiltonian describing the CQD system is given by [81–83, 147]

$$H_S = \varepsilon_b \mathcal{N}_b + \varepsilon_u \mathcal{N}_u + \kappa_c \mathcal{N}_b \mathcal{N}_u. \quad (32)$$

In Eq. (32),  $\varepsilon_\alpha > 0$  ( $\alpha = u, b$ ) denotes the single-particle energy level of the  $\alpha$ 'th QD, which are taken to be positive without loss of generality. Since the electron density in the dots is low, the occupancy is restricted to either zero or one [81–83, 142]. Consequently, the eigenstates of QD <sub>$\alpha$</sub>  are  $|0\rangle$  and  $|1\rangle$ , with eigenenergies 0 and  $\varepsilon_\alpha$ , respectively. The corresponding number operators for QD <sub>$\alpha$</sub>  are  $\mathcal{N}_b = d_b^\dagger d_b$  and  $\mathcal{N}_u = d_u^\dagger d_u$ , where  $d_b^\dagger$  ( $d_u$ ) and  $d_b$  ( $d_u$ ) denote the electron creation (annihilation) operators for the respective QD <sub>$\alpha$</sub> , obeying to the anti-commutation relations  $\{d_b, d_b^\dagger\} = 1 = \{d_u, d_u^\dagger\}$ . As the two QDs are strongly and capacitively coupled, the overall system Hamiltonian is diagonal in the eigenbasis of the individual QD. This can be represented by the tensor product of the number operator's eigenbasis of the coupled QDs. For convenience, the four eigenstates  $\{|0\rangle, |1\rangle\} \otimes \{|0\rangle, |1\rangle\}$ , are labeled by  $|A\rangle = |00\rangle$ ,  $|B\rangle = |10\rangle$ ,  $|C\rangle = |01\rangle$ ,  $|D\rangle = |11\rangle$  and their corresponding eigenenergies ( $\varepsilon_i$ ,  $i = A, B, C, D$ ) are  $\varepsilon_A = 0$ ,  $\varepsilon_B = \varepsilon_b$ ,  $\varepsilon_C = \varepsilon_u$  and  $\varepsilon_D = \varepsilon_b + \varepsilon_u + \kappa_c$  respectively [FIG. 4(b)]. Finally, the energy of the most excited state of the composite system is  $\varepsilon_u + \varepsilon_b + \kappa_c$ , where, we assume w.l.o.g,  $\varepsilon_b < \varepsilon_u$ .

The total Hamiltonian of all three reservoirs is given

by  $H_B = H_B^u + H_B^l + H_B^r$ . The QDs are weakly coupled to the reservoirs, allowing sequential tunnelling [20, 81–83, 151, 152]. The tunnel-coupled Hamiltonians characterised by the coupling constants  $t_k^{\alpha\lambda}$  are given by Eq. (6), which describes the tunnelling of a particle between the  $\alpha$ 'th QD and the reservoir  $\lambda$ . Furthermore, the transitions between  $|B\rangle \leftrightarrow |C\rangle$  and  $|A\rangle \leftrightarrow |D\rangle$  are prohibited due to the Coulomb blockade and the sequential tunnelling approximation [83, 148, 154]. So, there are in total four authorised transitions between the eigenstates of the composite system, and each of the three reservoirs *l*, *r*, and *u* controls two transitions, i.e.,  $|A\rangle \leftrightarrow |B\rangle$  and  $|C\rangle \leftrightarrow |D\rangle$  are triggered by leads *l* and/or *r*, while reservoir *u* governs the transitions between  $|A\rangle \leftrightarrow |C\rangle$  and  $|B\rangle \leftrightarrow |D\rangle$ , respectively. The transition energy between the eigenstates  $|i\rangle \rightarrow |j\rangle$  is defined as  $\omega_{ij} = \varepsilon_j - \varepsilon_i$ , where  $\varepsilon_i$  is the eigenenergy of  $H_S$  with the eigenstate  $\{|i\rangle\}$  and the four transition energies are, respectively  $\omega_{AB} = \varepsilon_L$ ,  $\omega_{AC} = \varepsilon_R$ ,  $\omega_{CD} = \varepsilon_L + \kappa_c$ , and  $\omega_{BD} = \varepsilon_R + \kappa_c$ .

The dynamics can be solved using the quantum master equation, similar to our previous two-terminal single-QD model. As usual, the state of the composite system is described by the reduced density matrix  $\rho_s(t) = \text{Tr}_B\{\rho_{\text{tot}}(t)\}$ , where  $\rho_{\text{tot}}(t)$  is the total system and the bath density matrix. The time evolution of  $\rho_s(t)$  is given by [74, 81, 83, 126] (See Appendix A):

$$\frac{d}{dt}\rho_s(t) = \sum_\lambda \mathcal{L}_\lambda[\rho_s(t)]; \quad \lambda = l, r, u. \quad (33)$$

where we utilise the strong coupling between the QDs, while maintaining the weak coupling between the system and its surrounding environment. This allows us to implement the BMS approximation and derive the above LME [Cf. Eq. (33)] solely based on the Hamiltonian  $H_S$  given in Eq. (32). As a consequence, the dissipation mechanism of each QD is influenced not only by its own bath but also by the interactions between QDs themselves. This becomes crucial for accurately characterising heat flow across a wide range of system parameters. The Lindblad super-operator  $\mathcal{L}_\lambda[\rho_s(t)]$  in Eq. (33) is defined in the Appendix A, and following the same treatment done in the single QD model, we can calculate the steady-state currents. The general analytical expressions of the steady-state energy and particle are already defined in Eq. (10), which yields the general heat current expression as

$$J_Q^\lambda = \sum_{\{\omega_{ij}\}} (\omega_{ij} - \mu_\lambda) \Gamma_{ij}^{\lambda+} = \sum_{\{\omega_{ji}\}} (\omega_{ji} - \mu_\lambda) \Gamma_{ji}^{\lambda-}, \quad (34)$$

where,  $\Gamma_{ij}^{\lambda+} = -\Gamma_{ji}^{\lambda-}$ . For this CQD-three terminal setup, at steady state ( $\dot{\rho}_i = 0$ ), the transition rates satisfy:

$$\begin{aligned} \Gamma_{AB}^{lr+} &= \Gamma_{BD}^{u+} = \Gamma_{DC}^{lr-} = \Gamma_{CA}^{u-} = \Gamma_{ABCD A} \equiv \Gamma_+; \\ \Gamma_{AC}^{u+} &= \Gamma_{CD}^{lr+} = \Gamma_{DB}^{u-} = \Gamma_{BA}^{lr-} = \Gamma_{ACDB A} \equiv \Gamma_-, \end{aligned} \quad (35)$$

implying  $\Gamma_+ = -\Gamma_-$ . With the help of Eq. (10), one can

verify

$$\begin{aligned} J_E^u &= \varepsilon_u \Gamma_+ + (\varepsilon_u + \kappa_c) \Gamma_- = \kappa_c \Gamma_+; \\ J_N^u &= \Gamma_{AC}^{u+} + \Gamma_{BD}^{u+} = \Gamma_+ + \Gamma_- = 0, \end{aligned} \quad (36)$$

as  $QD_u$  is coupled only to the lead  $u$ , resulting in  $J_N^u = 0$ . This immediately gives  $J_Q^u = J_E^u = \kappa_c \Gamma_+$ . As  $QD_u$  is only coupled with lead  $u$ , there will be no net particle current driven by  $u$  in the steady state, i.e.,  $J_N^u = 0$ . However,  $QD_b$  is simultaneously coupled with leads  $l$  and  $r$ , allowing particle flow across  $l$  and  $r$  in steady state. Since there is no external source or sink, the total energy and particle currents must be conserved in the steady state. Hence, we summarise our first set of results:

$$\sum_{\lambda=l,r,u} J_E^\lambda = 0, \quad \text{and} \quad \sum_{\lambda=l,r,u} J_N^\lambda = 0, \quad (37)$$

which yields

$$J_E^u = -J_E^{lr} = \kappa_c \Gamma_+; \quad \text{and} \quad J_N^l = -J_N^r. \quad (38)$$

The heat current is not conserved as  $J_Q^l + J_Q^r \equiv J_Q^{lr} \neq J_E^{lr} = -\kappa_c \Gamma_+$ .

## 2. Identifying thermodynamic forces

For the present model, the general form of the entropy production rate defined in Eq. (27) reads

$$\begin{aligned} \dot{\Sigma} &= -k_B[\beta_l J_E^l + \beta_r J_E^r + \beta_u J_E^u] \\ &\quad + k_B[\beta_l \mu_l J_N^l + \beta_r \mu_r J_N^r + \beta_u \mu_u J_N^u]. \end{aligned} \quad (39)$$

Since  $J_N^u = 0$ , Eq. (39) reduces to

$$\dot{\Sigma} = -k_B[\beta_l J_E^l + \beta_r J_E^r + \beta_u J_E^u] + k_B[\beta_l \mu_l J_N^l + \beta_r \mu_r J_N^r]. \quad (40)$$

Furthermore, both energy and particle currents are conserved in the steady state. This conservation follows directly from Eq. (37). These conditions lead to six equivalent representations of the entropy production rate. However, unlike the single-QD model, a subtlety arises in the present three-terminal setup. While the particle force can be identified uniquely, the energy biases are not unique and depend on the specific choice of independent energy currents used to express the entropy production rate. This non-uniqueness originates from the presence of two independent energy biases and one particle force in the three-terminal geometry. For the particle sector, one may choose  $J_N^l$  or  $J_N^r$  as the independent current; since they are equal in magnitude and opposite in direction, i.e.,  $J_N^l = -J_N^r$ . So, particle current can be identified unambiguously, and substituting this relation into Eq. (40) yields the following

$$\dot{\Sigma} = -k_B[\beta_l J_E^l + \beta_r J_E^r + \beta_u J_E^u] + \begin{cases} k_B(\beta_l \mu_l - \beta_r \mu_r) J_N^l, \\ \text{or} \\ k_B(\beta_r \mu_r - \beta_l \mu_l) J_N^r. \end{cases} \quad (41)$$

A comparison with the phenomenological form of the entropy production rate [cf. Eq. (1)], the particle force is then uniquely identified as

$$\mathcal{F}_N^l = -\mathcal{F}_N^r = k_B(\beta_l \mu_l - \beta_r \mu_r). \quad (42)$$

Since both definitions are thermodynamically equivalent, either choice of particle force may be employed. For the energy sector, the situation is a little more nuanced. Due to energy conservation  $J_E^l + J_E^r + J_E^u = 0$ , only two of the three energy currents are independent. Consequently, the entropy production rate can be expressed using different pairs of energy currents, leading to three distinct — yet physically equivalent — representations of the energy biases. To proceed, we fix the particle force as  $\mathcal{F}_N^l$  without loss of generality. Equation (41) then yields

$$\dot{\Sigma} = -k_B[\beta_l J_E^l + \beta_r J_E^r + \beta_u J_E^u] + J_N^l \mathcal{F}_N^l. \quad (43)$$

If we eliminate  $J_E^l$ , it gives the following results

$$\begin{aligned} \dot{\Sigma} &= k_B(\beta_l - \beta_r) J_E^r + k_B(\beta_l - \beta_u) J_E^u + J_N^l \mathcal{F}_N^l \\ &\equiv J_E^r \mathcal{F}_E^r + J_E^u \mathcal{F}_E^u + J_N^l \mathcal{F}_N^l \end{aligned} \quad (44)$$

which identifies the energy biases as

$$\mathcal{F}_E^r = k_B(\beta_l - \beta_r) \quad ; \quad \mathcal{F}_E^u = k_B(\beta_l - \beta_u). \quad (45)$$

Alternatively, eliminating  $J_E^r$  yields

$$\begin{aligned} \dot{\Sigma} &= k_B(\beta_r - \beta_l) J_E^l + k_B(\beta_r - \beta_u) J_E^u + J_N^l \mathcal{F}_N^l \\ &\equiv J_E^l \mathcal{F}_E^l + J_E^u \mathcal{F}_E^u + J_N^l \mathcal{F}_N^l \end{aligned} \quad (46)$$

leading to

$$\mathcal{F}_E^l = k_B(\beta_r - \beta_l) \quad ; \quad \mathcal{F}_E^u = k_B(\beta_r - \beta_u). \quad (47)$$

Finally, eliminating  $J_E^u$  yields

$$\mathcal{F}_E^l = k_B(\beta_u - \beta_l) \quad ; \quad \mathcal{F}_E^r = k_B(\beta_u - \beta_r) \quad (48)$$

These results show that the form of the energy biases depends on the chosen representation. Nevertheless, the thermodynamic behaviour remains invariant, since only two independent energy biases are sufficient to fully characterise the three-terminal setup. This non-uniqueness of thermodynamic forces and currents is not a mathematical inconsistency but an intrinsic feature of general three-terminal transport. Although explicit forms of forces depend on the choice of force-flux pairs used to express the entropy production rate, all such choices are thermodynamically equivalent and lead to the same physical behaviour. Accordingly, without loss of generality, we adopt the representation in Eq. (46), where the conjugate forces associated with the flux set  $\{J_E^l, J_E^u, J_N^l\}$  are given by Eq. (47). Alternative but equivalent representations may be constructed by choosing any two independent energy fluxes (e.g.,  $\{J_E^u, J_E^r\}$ ,  $\{J_E^u, J_E^l\}$ , or  $\{J_E^r, J_E^l\}$ ) together with one particle flux (either  $J_N^l$  or  $J_N^r$ ), and their

corresponding conjugate forces. Importantly, the quantities  $\{\mathcal{F}_E^u, \mathcal{F}_E^r, \mathcal{F}_N^r\}$  should not be interpreted as physical thermal or particle forces. Rather, they are *entropic energy* and *particle biases* — defined within the entropy representation — and are conjugate to the full set of fluxes  $\{J_E^u, J_E^r, J_N^r\}$ . In systems with a single force-flux pair, this distinction vanishes, and the entropic biases coincide uniquely with the physical thermodynamic forces.

However, the presence of three independent force–flux pairs complicates the thermodynamic analysis and can obscure the essential features of coupled transport. We therefore seek to reduce the three-terminal setup to an effective framework that captures core principles with minimal complexity. In the following, this reduction can be carried out systematically, making the model an ideal platform to study coupled energy–particle transport.

### 3. Reduction to an ideal model for coupled transport

Our objective is to effectively reduce the dimensionality of the model by imposing suitable constraints such that only two independent force–flux pairs remain. Since our primary interest lies in coupled transport involving two distinct transport processes, i.e., energy and particle transport, we must eliminate one of the energy force–flux pairs. This requires imposing an appropriate restriction on one of the energy biases, thereby reducing the three-terminal setup to an effective two-force framework suitable for analysing coupled transport [Fig. 5(a)]. This is analogous to the classical thermoelectric device [Fig. 5(b)]. Since we are interested in thermoelectric effects, we assume that the temperatures of the leads in the lower subsystem are equal. This implies  $\beta_l = \beta_r \equiv \beta$ . Under this condition, one of the entropic energy biases  $\mathcal{F}_E^l$  becomes zero, while the remaining two entropic biases are unambiguously reduced to the energy force  $\mathcal{F}_E^u = k_B(\beta - \beta_u)$  and a particle force  $\mathcal{F}_N^l = k_B\beta(\mu_l - \mu_r) := k_B\beta\Delta\mu$  as depicted in Fig. 5(a). The above choice of the parameters renders the present three-terminal CQD setup exactly equivalent to the well-known Sánchez–Büttiker model [18]. In this limit, the general expression for the entropy production rate in Eq. (46) simplifies to

$$\dot{\Sigma} = J_N^l \mathcal{F}_N^l + J_E^u \mathcal{F}_E^u. \quad (49)$$

It is important to emphasise that although Eq. (46) does not provide a unique representation of the entropy production rate, once one of the entropic biases vanishes (here  $\mathcal{F}_E^l = 0$ ), the remaining force–flux pairs acquire a direct physical interpretation. In this regime, Eq. (49) describes genuine coupled transport governed by well-defined thermodynamic energy and particle forces. Therefore, the above situation can be analysed in close analogy with the single-QD model. Consequently, all thermodynamic outcomes identified in the single-QD setup can also be recovered within the present

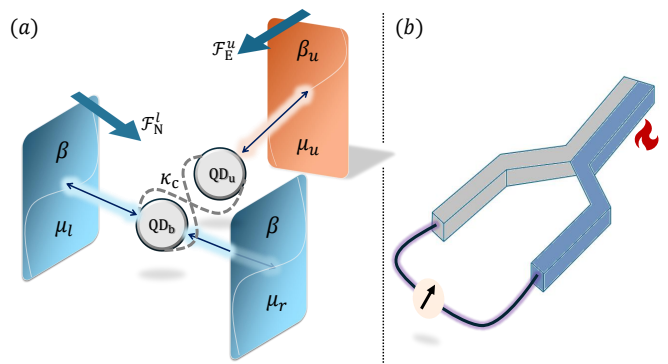


FIG. 5. (a) Schematic of the reduced CQD-three terminal setup as a model for a quantum thermoelectric device, (b) Classical thermoelectric device, from which the model is inspired.

reduced model. In this sense, the reduced CQD three-terminal configuration serves as a more convenient and appropriate framework for investigating coupled transport phenomena. In addition, similar to the minimal single-QD model, this reduced setup can operate as both a thermoelectric heat engine and a refrigerator. Due to these capabilities, the model is widely regarded as an efficient and experimentally relevant platform to study thermoelectric transport and energy conversion at the nanoscale [18, 20, 141, 146, 155].

Although this reduced model bears a close resemblance to the single-QD setup, an important distinction must be emphasised. In the earlier minimal models, the thermodynamic forces acted mutually parallel to each other. In contrast, as indicated by Eq. (49), the forces in the present reduced configuration are non-parallel, and the associated energy and particle currents are also non-parallel. This feature is precisely what makes the model analogous to classical thermoelectric devices, where electrical and thermal driving forces act along different directions. However, this characteristic also implies that the reduced model is not suitable for ICC, which, by definition, requires mutually parallel thermodynamic forces. Nevertheless, the reduced model remains highly effective for studying thermoelectric phenomena. It can capture all conventional thermoelectric effects, including Seebeck and Peltier effects, as well as their unconventional counterparts. However, these negative thermoelectric responses should not be interpreted as pseudo-ICC effects, since the driving forces are inherently non-parallel in this configuration. However, because of its clear physical interpretation and experimental relevance, this reduced model is one of the most suitable platforms for investigating thermoelectric transport.

Finally, we are left with a single remaining objective: to identify a model in which genuine ICC phenomena can be explored. Although the present reduced model does not permit this, the full CQD three-terminal framework offers additional flexibility and admits alternative reductions capable of exhibiting coupled transport under

mutually parallel forces. Accordingly, in the next section, we focus on constructing and analysing such an ideal reduced model, specifically designed to investigate the ICC effect.

## X. INVERSE CURRENT IN COUPLED TRANSPORT

To investigate ICC as a genuinely distinct effect, it is essential to impose the constraint such that it yields a reduced model with two mutually parallel forces. This requirement can be fulfilled naturally if both the energy and particle forces are associated with the same reservoir. In the present formulation, following Eq. (46), the single particle force  $\mathcal{F}_N^l$  is already associated with the left lead. Consequently, to obtain mutually parallel forces, the remaining energy force must also be associated with the left lead. This can be achieved by imposing a thermodynamic constraint in which the other energy force,  $\mathcal{F}_E^u$ , vanishes. From Eq. (47), this condition is satisfied by  $\beta_r = \beta_u = \beta$ , which means that the left and upper reservoirs are held at the same temperatures. Under this condition, the general CQD three-terminal setup reduces to an effective two-force coupled-transport system, in which the entropy production rate can be expressed in terms of mutually parallel energy and particle forces, as

$$\dot{\Sigma} = J_E^l \mathcal{F}_E^l + J_N^l \mathcal{F}_N^l, \quad (50)$$

where the two real *thermodynamic forces* are defined as  $\mathcal{F}_E^l = k_B(\beta_l - \beta)$  and  $\mathcal{F}_N^l = k_B(\beta_l \mu_l - \beta \mu_r)$ , respectively [Fig. 6(a)]. Without loss of generality, we consider that both forces are mutually parallel and satisfy  $\mathcal{F}_E^l > 0$  and  $\mathcal{F}_N^l > 0$ . In this condition, either  $J_E^l$  or  $J_N^l$  may flow against both forces. The resulting negative contribution to the entropy production rate can be compensated by the remaining current flowing along the forces, such that the total entropy production remains non-negative  $\dot{\Sigma} \geq 0$ . Accordingly, Fig. 6(a) illustrates the ideal configuration for ICC, where one current is driven simultaneously against two mutually parallel thermodynamic forces, yet the second law of thermodynamics is fully satisfied.

Interestingly, the resulting expression for the entropy production rate is formally identical to that of the minimal two-terminal single-QD model. Thus, one expects the standard thermodynamic cross-effects of coupled transport—such as the Seebeck and Peltier effects—to be observed within this reduced framework. Moreover, in the minimal single-QD model and the Sánchez-Büttiker configuration, the system can operate either as a thermoelectric heat engine or as a refrigerator. However, these conventional cross-effects have already been extensively studied [15–20, 22, 23, 84–86]. We are interested here in whether the present reduced model can support the emergence of ICC, a genuinely distinct and counter-intuitive thermodynamic phenomenon, and under what

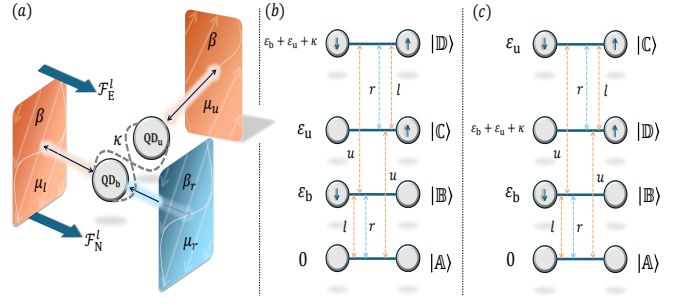


FIG. 6. (a) Ideal schematic of three-terminal CQD setup for realising ICC effect. The energy level diagram of the composite system eigenstates for (b)  $\kappa > 0$  and (c)  $\kappa < 0$ ; but  $|\kappa| > \epsilon_b$ .

conditions such an effect can be realised. In the single-QD model, although the thermodynamic forces are mutually parallel, the strict constraint linking the energy and particle currents precludes the emergence of either pseudo-ICC or genuine ICC behaviour, rendering inverse currents impossible. Since the present reduced model yields an entropy production rate formally identical to that of the two-terminal single-QD setup, a natural question arises: *does this model necessarily inherit the same limitations, or can it support ICC behaviour despite this apparent equivalence?*

Despite their formal equivalence in force–flux space, the two models differ fundamentally in structure and dynamics. The previous model consists of a single QD, acting as a TLS, whereas the reduced model considered here is based on a CQD architecture, comprising two strongly and capacitively coupled QDs. This structural complexity significantly alters the internal dynamics of the system. Consequently, the solution of the LME [cf. Eq. (33)] for the CQD system yields a dynamical behaviour that is qualitatively distinct from that of the single-QD model. A detailed and comprehensive analysis of this CQD setup has already been carried out in Ref. [43]. The steady-state energy and particle currents in this case are given by

$$\begin{aligned} J_E^l &= \epsilon_b \Gamma_{AB}^{l+} + (\epsilon_b + \kappa) \Gamma_{CD}^{l+} = \epsilon_b J_N^l + \kappa \Gamma_{CD}^{l+}; \\ J_N^l &= (\Gamma_{AB}^{l+} + \Gamma_{CD}^{l+}) \end{aligned} \quad (51)$$

where the  $\Gamma_{ij}^{\lambda+}$  stands for the net excitation rates from the state  $|i\rangle$  to  $|j\rangle$  induced by reservoir  $\lambda$  [Cf. Eq. (11)]. It is evident from Eq. (51) that the energy and particle currents in this model are no longer proportional to each other, i.e.,  $J_E^l \neq \epsilon J_N^l$ . In this case, an additional term appears that depends on the strength of the inter-dot interaction  $\kappa$ . The presence of this new term may lead to the possibility of realising a genuine ICC effect within the present model. A detailed analysis in Ref. [43] shows that for positive  $\kappa$ , the transport remains qualitatively similar to the single-QD case and no inverse-current behaviour is observed. In contrast, negative inter-dot interactions can open a qualitatively new transport regime. However,

a negative  $\kappa$  alone is not sufficient to guarantee ICC. Rather, ICC becomes feasible *iff* the symmetry between energy and particle exchange is broken. This occurs when the ordering of the system eigenstates  $|\mathbb{C}\rangle$  and  $|\mathbb{D}\rangle$  is inverted, which requires  $\varepsilon_b + \kappa < \varepsilon_b$ .

The remaining question is how to break the symmetry between energy and particle exchange. As discussed above, this requires a negative interaction parameter  $\kappa$ , corresponding to an effective attraction between the QDs. However, in the standard three-terminal CQD model, the interdot Coulomb interaction is inherently repulsive, yielding only  $\kappa > 0$ . To overcome this limitation, we modified the model to allow for effective attractive interactions. Specifically, we consider spin-polarised electronic reservoirs instead of spinless ones. While spinless electrons permit only repulsive interdot interaction, spin-polarised reservoirs [82, 135] enable more general interaction scenarios and allow for  $\kappa < 0$ . In this setup, QD<sub>b</sub> is coupled to spin-down ( $\downarrow$ ) electronic reservoirs, whereas QD<sub>u</sub> is coupled to a spin-up ( $\uparrow$ ) reservoir [FIG. 6(a)]. Under these assumptions, the Hamiltonian of the coupled QD system takes the form

$$H_S = \varepsilon_b \mathcal{N}_{b\downarrow} + \varepsilon_u \mathcal{N}_{u\uparrow} + \kappa_c \mathcal{N}_{b\downarrow} \mathcal{N}_{u\uparrow} + \kappa_s \sigma_{b\downarrow}^z \sigma_{u\uparrow}^z. \quad (52)$$

Here,  $\varepsilon_\alpha > 0$  ( $\alpha = b, u$ ) is the single-particle energy level of the  $\alpha$ 'th QD. Due to the low electron density [81–83, 142], each dot can host at most one electron. So, the eigenstates of QD<sub>b(u)</sub> are  $|0\rangle$  and  $|\downarrow\rangle$  ( $|\uparrow\rangle$ ), with energies 0 and  $\varepsilon_b$  ( $\varepsilon_u$ ), respectively. The corresponding number operators are  $\mathcal{N}_{b\downarrow} = d_{b\downarrow}^\dagger d_{b\downarrow}$  and  $\mathcal{N}_{u\uparrow} = d_{u\uparrow}^\dagger d_{u\uparrow}$ , where  $d_{\alpha\sigma}^\dagger$  ( $d_{\alpha\sigma}$ ) creates (annihilates) an electron with spin  $\sigma = \uparrow, \downarrow$  in the dot  $\alpha$ . These operators satisfy the canonical anti-commutation relations  $d_{\alpha\sigma}, d_{\alpha'\sigma'}^\dagger = \delta_{\alpha\alpha'} \delta_{\sigma\sigma'}$ . The spin–spin interaction term [156] is expressed by  $\sigma_{b\downarrow}^z = 1 - 2\mathcal{N}_{b\downarrow}$  and  $\sigma_{u\uparrow}^z = 2\mathcal{N}_{u\uparrow} - 1$ , with the standard relations  $\sigma_{b\downarrow}^z |\downarrow\rangle = -|\downarrow\rangle$  and  $\sigma_{u\uparrow}^z |\uparrow\rangle = +|\uparrow\rangle$ . Due to strong capacitive coupling [82, 83, 135], the system Hamiltonian  $H_S$  is diagonal in the tensor-product eigenbasis of the individual QD number operators. The four eigenstates  $|0\rangle, |\downarrow\rangle \otimes |0\rangle, |\uparrow\rangle$  are labelled as  $|\mathbb{A}\rangle = |00\rangle$ ,  $|\mathbb{B}\rangle = |\downarrow 0\rangle$ ,  $|\mathbb{C}\rangle = |0 \uparrow\rangle$ ,  $|\mathbb{D}\rangle = |\downarrow \uparrow\rangle$  with corresponding energies  $\varepsilon_{\mathbb{A}} = 0$ ,  $\varepsilon_{\mathbb{B}} = \varepsilon_b$ ,  $\varepsilon_{\mathbb{C}} = \varepsilon_u$ , and  $\varepsilon_{\mathbb{D}} = \varepsilon_b + \varepsilon_u + \kappa$  [FIG. 6(b), 6(c)]. The total interaction strength is given by  $\kappa = \kappa_c - \kappa_s$ , where both  $\kappa_c$  and  $\kappa_s$  are positive and w.l.o.g, we assume  $\varepsilon_b < \varepsilon_u$ . As a result,  $\kappa$  can be repulsive ( $\kappa > 0$ ) or attractive ( $\kappa < 0$ ). When  $\kappa < 0$  and  $|\kappa| > \varepsilon_b$ , the order of the energy of the states  $|\mathbb{C}\rangle$  and  $|\mathbb{D}\rangle$  is inverted [FIG. 6(c)], signalling a breakdown of the symmetry between energy and particle exchange. While an isolated electron generates a repulsive Coulomb interaction, placing it in an appropriately engineered environment can effectively invert the sign of this interaction, making it attractive to other electrons [157–160]. This effective attraction was experimentally demonstrated by Hamo *et al.* [157] using a carbon-nanotube double QD coupled to a charge qubit. In this configuration, the qubit's oscillating polarisation

field “dresses” the electron–electron interaction, stabilising doubly occupied states relative to singly occupied ones [157–160], as schematically shown in Fig. 6(c).

The central result is that the condition  $-\kappa > \varepsilon_b > 0$  is required for the appearance of ICC in both energy and particle currents. This inequality corresponds to an interchange of the energy levels associated with the states  $|0 \uparrow\rangle$  ( $|\mathbb{C}\rangle$ ) and  $|\downarrow \uparrow\rangle$  ( $|\mathbb{D}\rangle$ ). For repulsive interdot interactions ( $\kappa > 0$ ), the eigenstates are ordered such that particle excitation (de-excitation) necessarily implies energy excitation (de-excitation), as shown in Fig. 6(b). In contrast, when the attractive interaction satisfies  $-\kappa > \varepsilon_b > 0$ , the eigenstate ordering is inverted [Fig. 6(c)]. A particle excitation process,  $|0 \uparrow\rangle \rightarrow |\downarrow \uparrow\rangle$ , is then accompanied by energetic de-excitation, and vice versa. This breaking of symmetry between energy and particle exchange is the key mechanism that allows one current to flow against its conjugate thermodynamic force while remaining fully consistent with the second law. Notably, Wang *et al.* [42] also identified a kind of symmetry-breaking criterion for classical Hamiltonian systems, suggesting that symmetry breaking is a general prerequisite for ICC in both quantum and classical regimes. In the present CQD model, an attractive interdot interaction ( $\kappa < 0$ ) [157, 158] provides the necessary condition, while the inequality serves as a sufficient criterion for the implementation of ICC.

A natural question is whether the necessary and sufficient conditions identified here for genuine ICC are specific to the present reduced model, or whether they extend to more general frameworks. Several studies have reported ICC-like behaviour in alternative CQD configurations, particularly in “two-terminal” setups where both dots are symmetrically coupled to the same pair of reservoirs [131, 137]. While such models may appear minimal, their dynamics are in fact more complex: each dot is simultaneously coupled to multiple reservoirs, often to the same leads, in addition to being strongly and capacitively coupled to each other. This substantially increases the complexity compared to the present three-terminal framework. Crucially, the reported inverse currents in these two-terminal models are typically defined with respect to thermodynamic gradients (e.g.,  $\Delta T$  or  $\Delta\mu$ ), rather than the true conjugate thermodynamic forces that enter the entropy production rate. Since gradients and forces are not necessarily equivalent, inverse transport relative to gradients alone does not guarantee genuine ICC. ICC must be defined through the force–flux structure of entropy production rate. In particular, the central role of symmetry breaking between energy and particle transport—identified here as the key ingredient for ICC — suggests that similar conditions are likely to govern the emergence of ICC in other CQD architectures. Following a similar analysis to that presented here, one can, in principle, test the validity of this conjecture in a two-terminal CQD setup as well. However, a detailed investigation of this case lies beyond the scope of the present review and is therefore left as an open and stimulating problem for interested readers and for future stud-

ies on ICC.

To conclude, a genuine ICC can be achieved in both energy- and spin-polarised particle currents when the two mutually parallel thermodynamic forces are positive. This opens up promising avenues for unconventional autonomous nano-thermoelectric engines and refrigerators based on ICC effects in coupled QD systems. In particular, our analysis reveals that attractive interactions between QDs constitute a necessary requirement for realising such autonomous quantum thermal machines [157–160]. Furthermore, the spin-resolved nature of the transport highlights the potential for more versatile spin-thermoelectric devices beyond traditional designs, with their novelty rooted in the counterintuitive thermodynamic behaviour of inverse currents. Interestingly, an autonomous circular heat engine inspired by ICC in classical systems [42] has recently been proposed by Benenti et al. [161]. We therefore expect that the present findings will play an important role in the advancement of ICC-assisted autonomous quantum thermal devices in stimulating further experimental and theoretical exploration in this direction.

## XI. SUMMARY AND OUTLOOK

In summary, this review presents a comprehensive account of the thermodynamics of quantum-coupled transport (QCT). We begin with single transport processes and progress to coupled transport, highlighting the richer thermodynamic behaviour that emerges. Starting from a single quantum dot (QD), we examine the thermodynamic consequences of coupled energy and particle transport and emphasise the distinction between conventional thermodynamic cross-effects and inverse currents in coupled (ICC) transport. We then introduce a three-terminal coupled quantum dot (CQD) framework, analyse thermoelectric phenomena in a reduced configuration that reproduces the minimal single-QD model, and propose an alternative reduced model, derived from the general CQD architecture, to investigate genuine ICC effects. This underscores the importance of QD-based platforms for probing non-equilibrium thermodynamics and summarises the key outcomes of this review along the future roadmap.

- *Identification of force–flux pairs:* We presented a detailed thermodynamic analysis of how relevant force–flux pairs can be systematically identified by examining the form of entropy production rate in the near-equilibrium regime. This methodology is general and can be straightforwardly extended to more complex systems, where a force–flux description may reveal richer thermodynamic behaviour associated with multidimensional transport processes.
- *Single transport processes as a foundation:* We began with the simplest form of transport, namely

a single transport process. Such processes are inherently simple, leading to currents that necessarily flow along the direction of the applied thermodynamic force. This restriction is relaxed beyond the near-equilibrium regime, giving rise to phenomena such as absolute negative mobility (ANM) [52–56, 162, 163]. Although single transport processes do not exhibit particularly rich thermodynamic features, they serve as a conceptual foundation for understanding more complex coupled transport phenomena beyond equilibrium.

- *Force versus gradient:* A subtle yet pertinent point addressed in this review is the distinction between thermodynamic forces and gradients, and which of these quantities truly characterise the thermodynamics of current flow. Although these terms are often used interchangeably, they are not, in general, thermodynamically equivalent. As demonstrated throughout this review, the correct thermodynamic description is rooted in the entropy production rate, where each flux is paired with its conjugate thermodynamic force. This establishes the thermodynamic force and not the mere gradient as the fundamental driver of transport. While gradients may coincide with thermodynamic forces in special cases and thus serve as useful proxies, a rigorous and consistent analysis, — particularly in multi-terminal or complex systems — must be formulated in terms of properly defined thermodynamic forces.
- *Coupled transport with single QD:* We then turn our attention to the central theme of this perspective article — coupled transport, with particular emphasis on QCT involving energy and particle currents. Starting from the minimal setup of a single QD tunnel-coupled to two fermionic reservoirs, we systematically explored all thermodynamically allowed transport regimes. Within this framework, we discuss fundamental thermoelectric effects, such as the Seebeck and Peltier effects, as well as the operating principles of thermoelectric heat engines and refrigerators. In particular, all these functionalities already arise in this single-QD model. However, despite its conceptual simplicity, the model is not suited to capture counterintuitive transport phenomena such as ICC.
- *Inverse current phenomena:* A central result of this review is the detailed analysis of the ICC phenomena. We establish ICC as a rare and counterintuitive thermodynamic effect — fully consistent with the second law, yet fundamentally distinct from conventional cross-effects — and clarify the conceptual and physical differences between these two effects. While a minimal single-QD setup cannot support genuine ICC, we show that the CQD framework provides the necessary freedom to de-

sign configurations in which ICC can be rigorously explored.

- *Three-terminal CQD model and thermoelectric effects:* In the later part of this review, we examine the three-terminal CQD model and establish it as an ideal platform for studying coupled transport. We present a comprehensive thermodynamic analysis, with particular emphasis on the careful identification of appropriate force–flux pairs. By imposing suitable physical constraints, we show that the CQD model can be systematically reduced to the well-known Sánchez–Büttiker model, which is directly analogous to classical thermoelectric devices and captures standard thermodynamic cross-effects [15–23, 84–86, 141]. We further demonstrate that this reduced model closely mimics the minimal single–QD setup, confirming its effectiveness as a realistic model for thermoelectric transport studies.
- *Toward a genuine ICC and autonomous device:* Finally, we propose a special reduced model — derived from the general three-terminal CQD architecture — in which genuine ICC emerges as a novel feature of coupled transport [42, 43]. This is achieved by breaking the symmetry between the energy and particle channels through an at-

tractive interaction between the QDs mediated by spin-polarised fermionic reservoirs. This symmetry breaking reshapes the transport profile and enables true ICC. While a detailed quantitative analysis is discussed elsewhere [43], the model provides a promising platform for exploring autonomous thermoelectric heat engines and refrigerators powered by ICC phenomena.

We conclude with a summary of coupled transport processes with the aim of clarifying the key concepts and thermodynamic principles underlying thermoelectric devices. Beyond consolidating existing knowledge, we hope that the perspectives presented here — particularly the role of inverse currents — will inspire future efforts to design more efficient autonomous thermoelectric engines and refrigerators. In this way, this review seeks to make a modest, yet meaningful contribution to both the theoretical understanding and practical realisation of coupled transport phenomena.

## ACKNOWLEDGMENTS

AG acknowledges IITK for infrastructure and partial financial support. SG acknowledges the Ministry of Education, Government of India, for the Prime Minister Research Fellowship (PMRF).

- 
- [1] H. B. Callen, *thermodynamics and an introduction to thermostatistics* (wiley, new york, 1985).
  - [2] D. Kondepudi and I. Prigogine, *Modern Thermodynamics*, 2nd ed. (John Wiley & Sons Ltd, Chichester, 2015).
  - [3] J. Gemmer, M. Michel, and G. Mahler, *Quantum Thermodynamics*, 2nd ed. (Springer-Verlag, Berlin Heidelberg, 2009).
  - [4] S. Vinjanampathy and J. Anders, Quantum thermodynamics, *Contemp. Phys.* **57**, 1 (2016).
  - [5] S. Datta, *Electronic Transport in Mesoscopic Systems*, Cambridge Studies in Semiconductor Physi (Cambridge University Press, 1997).
  - [6] Y. Imry, *Introduction to Mesoscopic Physics* (Oxford University Press, 2002).
  - [7] S. R. de Groot and P. Mazur, *non-equilibrium thermodynamics* (north-holland, amsterdam, 1962).
  - [8] Y. Nazarov and Y. Blanter, *Quantum Transport: Introduction to Nanoscience* (Cambridge University Press, 2009).
  - [9] M. Di Ventra, *Electrical Transport in Nanoscale Systems* (Cambridge University Press, 2008).
  - [10] U. Seifert, stochastic thermodynamics, fluctuation theorems and molecular machines, reports on progress in physics **75**, 126001 (2012).
  - [11] H. B. Callen, The application of onsager’s reciprocal relations to thermoelectric, thermomagnetic, and galvanomagnetic effects, *Phys. Rev.* **73**, 1349 (1948).
  - [12] I. Prigogine, *Introduction to Thermodynamics of Irreversible Processes*, 2nd ed. (Interscience Publishers, New York London, 1961).
  - [13] L. Onsager, Reciprocal relations in irreversible processes. i., *Phys. Rev.* **37**, 405 (1931).
  - [14] L. Onsager, Reciprocal relations in irreversible processes. ii., *Phys. Rev.* **38**, 2265 (1931).
  - [15] J. Monsel, J. Schulenburg, T. Baquet, and J. Splettstoesser, Geometric energy transport and refrigeration with driven quantum dots, *Phys. Rev. B* **106**, 035405 (2022).
  - [16] M. Josefsson, A. Svilans, A. M. Burke, E. A. Hoffmann, S. Fahlvik Svensson, M. Leijnse, and H. Linke, A quantum-dot heat engine operating close to the thermodynamic efficiency limits, *Nature Nanotechnology* **13**, 920 (2018).
  - [17] D. Prete, P. A. Erdman, S. Demesmaeker, and B. Sothmann, Thermoelectric conversion at 30 k in inas/inp nanowire quantum dots, *Nano Letters* **19**, 3033 (2019).
  - [18] R. Sánchez and M. Büttiker, Optimal energy quanta to current conversion, *Phys. Rev. B* **83**, 085428 (2011).
  - [19] Y. Zhang, G. Lin, and J. Chen, Three-terminal quantum-dot refrigerators, *Phys. Rev. E* **91**, 052118 (2015).
  - [20] H. Thierschmann, R. Sánchez, B. Sothmann, F. Arnold, C. Heyn, W. Hansen, H. Buhmann, and L. W. Molenkamp, Three-terminal energy harvester with coupled quantum dots, *Nature Nanotechnology* **10**, 854 (2015).
  - [21] H. Thierschmann, R. Sánchez, B. Sothmann, H. Buhmann, and L. W. Molenkamp, Thermoelectrics with

- coulomb-coupled quantum dots, *Comptes Rendus. Physique* **17**, 1109 (2016).
- [22] P. A. Erdman, F. Mazza, R. Bosisio, G. Benenti, R. Fazio, and F. Taddei, Thermoelectric properties of an interacting quantum dot based heat engine, *Phys. Rev. B* **95**, 245432 (2017).
- [23] S. Jurgens, F. Haupt, M. Moskalets, and J. Splettstoesser, Thermoelectric performance of a driven double quantum dot, *Physical Review B* **87**, 245423 (2013).
- [24] T. J. Seebeck, Magnetische polarisation der metalle und erze durch temperatur-differenz, *Abhandlungen der Königlichten Akademie der Wissenschaften zu Berlin*, 265 (1822).
- [25] W. Thomson, On the dynamical theory of heat, *Transactions of the Royal Society of Edinburgh* **21**, 123 (1856).
- [26] S. R. de Groot and P. Mazur, *Non-Equilibrium Thermodynamics* (Dover Publications, New York, 1984).
- [27] G. D. Mahan and J. O. Sofo, The best thermoelectric, *Proceedings of the National Academy of Sciences* **93**, 7436 (1996).
- [28] M. Esposito, K. Lindenberg, and C. Van den Broeck, Thermoelectric efficiency at maximum power in a quantum dot, *New Journal of Physics* **12**, 013013 (2010).
- [29] S. F. Svensson, A. I. Persson, E. A. Hoffmann, N. Nakpathomkun, H. A. Nilsson, H. Q. Xu, L. Samuelson, and H. Linke, Lineshape of the thermopower of quantum dots, *New Journal of Physics* **14**, 033041 (2012).
- [30] R. S. Whitney, Most efficient quantum thermoelectric at finite power output, *Physical Review Letters* **112**, 130601 (2014).
- [31] J. C. A. Peltier, Nouvelles expériences sur la caloricit  des courants  lectriques, *Annales de Chimie et de Physique* **56**, 371 (1834).
- [32] A. N. Jordan, B. Sothmann, R. S nchez, and M. B ttiker, Powerful and efficient energy harvester with resonant-tunneling quantum dots, *Phys. Rev. B* **87**, 075312 (2013).
- [33] B. Sothmann, R. S nchez, and A. N. Jordan, Quantum dots as thermal rectifiers, *Nanotechnology* **23**, 365101 (2012).
- [34] S. Donsa, S. Andergassen, and K. Held, Double quantum dot as a minimal thermoelectric generator, *Phys. Rev. B* **89**, 125103 (2014).
- [35] A.-M. Dar  and P. Lombardo, Powerful coulomb-drag thermoelectric engine, *Phys. Rev. B* **96**, 115414 (2017).
- [36] A. Singha, A realistic non-local heat engine based on Coulomb-coupled systems, *Journal of Applied Physics* **127**, 234903 (2020).
- [37] P. A. Erdman, B. Bhandari, R. Fazio, J. P. Pekola, and F. Taddei, Absorption refrigerators based on coulomb-coupled single-electron systems, *Phys. Rev. B* **98**, 045433 (2018).
- [38] A.-M. Dar , Comparative study of heat-driven and power-driven refrigerators with coulomb-coupled quantum dots, *Phys. Rev. B* **100**, 195427 (2019).
- [39] S. Mukherjee, B. De, and B. Muralidharan, Three-terminal vibron-coupled hybrid quantum dot thermoelectric refrigeration, *Journal of Applied Physics* **128**, 234303 (2020).
- [40] A. Barman, S. Halder, S. K. Varshney, G. Dutta, and A. Singha, Realistic nonlocal refrigeration engine based on coulomb-coupled systems, *Phys. Rev. E* **103**, 012131 (2021).
- [41] R. D. Mayrhofer, C. Elouard, J. Splettstoesser, and A. N. Jordan, Stochastic thermodynamic cycles of a mesoscopic thermoelectric engine, *Phys. Rev. B* **103**, 075404 (2021).
- [42] J. Wang, G. Casati, and G. Benenti, Inverse currents in hamiltonian coupled transport, *Phys. Rev. Lett.* **124**, 110607 (2020).
- [43] S. Ghosh, N. Gupt, and A. Ghosh, Inverse current in coupled transport: A quantum thermodynamic model (2026), (under communication):(under communication).
- [44] J. Fourier, *the analytical theory of heat* (cambridge university press, cambridge, 1822).
- [45] A. Fick, on liquid diffusion, *philosophical magazine* **10**, 30 (1855).
- [46] G. S. Ohm, *die galvanische kette mathematisch bearbeitet* (riegel und wie ner, berlin, 1827).
- [47] N. W. Ashcroft and N. D. Mermin, *solid state physics* (holt, rinehart and winston, new york, 1976).
- [48] J. M. Ziman, *Principles of the Theory of Solids* (Cambridge University Press, 1972).
- [49] S. Datta, *Electronic Transport in Mesoscopic Systems* (Cambridge University Press, 1995).
- [50] I.  uti , J. Fabian, and S. Das Sarma, spintronics: fundamentals and applications, reviews of modern physics **76**, 323 (2004).
- [51] L. D. Landau and E. M. Lifshitz, *fluid mechanics*, course of theoretical physics, Vol. 6 (pergamon press, oxford, 1987).
- [52] L. Machura, M. Kostur, P. Talkner, J. Luczka, and P. H nggi, Absolute negative mobility induced by thermal equilibrium fluctuations, *Phys. Rev. Lett.* **98**, 040601 (2007).
- [53] P. Reimann, Brownian motors: noisy transport far from equilibrium, *Physics Reports* **361**, 57 (2002).
- [54] R. Eichhorn, P. Reimann, and P. H nggi, Brownian motion exhibiting absolute negative mobility, *Phys. Rev. Lett.* **88**, 190601 (2002).
- [55] J. Nagel, D. Speer, T. Gaber, A. Sterck, R. Eichhorn, P. Reimann, K. Ilin, M. Siegel, D. Koelle, and R. Kleiner, Observation of negative absolute resistance in a josephson junction, *Phys. Rev. Lett.* **100**, 217001 (2008).
- [56] J.-X. Zhu and A. V. Balatsky, Absolute negative mobility in quantum transport, *Physical Review B* **70**, 195107 (2004).
- [57] R. A. H pfel, J. Shah, P. A. Wolff, and A. C. Gossard, Negative absolute mobility of minority electrons in gaas quantum wells, *Phys. Rev. Lett.* **56**, 2736 (1986).
- [58] B. J. Keay, S. Zeuner, S. J. Allen, K. D. Maranowski, A. C. Gossard, U. Bhattacharya, and M. J. W. Rodwell, Dynamic localization, absolute negative conductance, and stimulated, multiphoton emission in sequential resonant tunneling semiconductor superlattices, *Phys. Rev. Lett.* **75**, 4102 (1995).
- [59] A. Sarracino, F. Cecconi, A. Puglisi, and A. Vulpiani, Nonlinear response of inertial tracers in steady laminar flows: Differential and absolute negative mobility, *Phys. Rev. Lett.* **117**, 174501 (2016).
- [60] P. K. Ghosh, P. H nggi, F. Marchesoni, and F. Nori, Giant negative mobility of janus particles in a corrugated

- channel, *Phys. Rev. E* **89**, 062115 (2014).
- [61] D. Reguera, A. Luque, P. S. Burada, G. Schmid, J. M. Rubí, and P. Hänggi, Entropic splitter for particle separation, *Phys. Rev. Lett.* **108**, 020604 (2012).
- [62] A. Ślapiak, J. Luczka, P. Hänggi, and J. Spiechowicz, Tunable mass separation via negative mobility, *Phys. Rev. Lett.* **122**, 070602 (2019).
- [63] B. Cleuren and C. V. den Broeck, Ising model for a brownian donkey, *Europhysics Letters* **54**, 1 (2001).
- [64] B. Cleuren and C. Van den Broeck, Random walks with absolute negative mobility, *Phys. Rev. E* **65**, 030101 (2002).
- [65] B. S. Dandogbessi and A. Kenfack, Absolute negative mobility induced by potential phase modulation, *Phys. Rev. E* **92**, 062903 (2015).
- [66] J. Spiechowicz, P. Hänggi, and J. Luczka, Coexistence of absolute negative mobility and anomalous diffusion, *New Journal of Physics* **21**, 083029 (2019).
- [67] A. Ros, R. Eichhorn, J. Regtmeier, T. T. Duong, P. Reimann, and D. Anselmetti, Absolute negative particle mobility, *Nature* **436**, 928 (2005).
- [68] G. Benenti, G. Casati, K. Saito, and R. Whitney, Fundamental aspects of steady-state conversion of heat to work at the nanoscale, *Physics Reports* **694**, 1 (2017), fundamental aspects of steady-state conversion of heat to work at the nanoscale.
- [69] J. P. Pekola and B. Karimi, Colloquium: Quantum heat transport in condensed matter systems, *Rev. Mod. Phys.* **93**, 041001 (2021).
- [70] R. Sánchez and B. Sothmann, Thermoelectric transport of mesoscopic conductors coupled to voltage and temperature probes, *Physical Review B* **99**, 245304 (2019).
- [71] L. P. Kouwenhoven, C. M. Marcus, P. L. McEuen, S. Tarucha, R. M. Westervelt, and N. S. Wingreen, Electron transport in quantum dots, *NATO ASI Series E* **345**, 105 (1997).
- [72] W. G. van der Wiel, S. De Franceschi, J. M. Elzerman, T. Fujisawa, S. Tarucha, and L. P. Kouwenhoven, Electron transport through double quantum dots, *Reviews of Modern Physics* **75**, 1 (2002).
- [73] H. Linke and T. E. Humphrey, Harnessing non-equilibrium fluctuations for thermoelectric devices, *Physics Today* **68**, 32 (2015).
- [74] H.-P. Breuer and F. Petruccione, *The Theory of Open Quantum Systems* (Oxford University Press, 2007).
- [75] W. H. Louisell, *Quantum Statistical Properties of Radiation*, A Wiley-Interscience publication (Wiley, New York, 1990).
- [76] H. Carmichael, *An Open Systems Approach to Quantum Optics* (Springer-Verlag, Berlin Heidelberg, 1993).
- [77] D. Gelbwaser-Klimovsky, W. Niedenzu, and G. Kurizki, Thermodynamics of quantum systems under dynamical control, *Adv. At. Mol. Opt. Phys.* **64**, 329 (2015).
- [78] G. Kurizki and A. G. Kofman, *Thermodynamics and Control of Open Quantum Systems* (Cambridge University Press, 2022).
- [79] A. Ghosh, C. L. Latune, L. Davidovich, and G. Kurizki, Catalysis of heat-to-work conversion in quantum machines, *Proc. Natl. Acad. Sci. U.S.A.* **114**, 12156 (2017).
- [80] N. Gupt, S. Bhattacharyya, B. Das, S. Datta, V. Mukherjee, and A. Ghosh, Floquet quantum thermal transistor, *Phys. Rev. E* **106**, 024110 (2022).
- [81] N. Gupt, S. Ghosh, and A. Ghosh, Top-ranked cycle flux network analysis of molecular photocells, *Phys. Rev. E* **108**, 034305 (2023).
- [82] N. Gupt, S. Ghosh, and A. Ghosh, Graph theoretic analysis of three-terminal quantum dot thermocouples: Onsager relations and spin-thermoelectric effects, *Phys. Rev. B* **109**, 125124 (2024).
- [83] S. Ghosh, N. Gupt, and A. Ghosh, Universal behavior of the coulomb-coupled fermionic thermal diode, *Entropy* **24** (2022).
- [84] G. Jaliel, S. Demesmaecker, and B. Sothmann, Experimental realization of a quantum-dot energy harvester, *Physical Review Letters* **123**, 117701 (2019).
- [85] N. Nakpathomkun, H. Q. Xu, and H. Linke, Thermoelectric efficiency at maximum power in low-dimensional systems, *Phys. Rev. B* **82**, 235428 (2010).
- [86] M. Josefsson, B. Sothmann, M. Leijnse, and H. Linke, Optimal power and efficiency of single quantum dot heat engines: theory and experiment, *Physical Review B* **99**, 235432 (2019).
- [87] C. McConnell and A. Nazir, Strong coupling in thermoelectric nanojunctions: A reaction coordinate framework, *New Journal of Physics* **24**, 025002 (2022).
- [88] P. Strasberg, G. Schaller, T. Brandes, and M. Esposito, Thermodynamics of a physical model implementing a maxwell demon, *Phys. Rev. Lett.* **110**, 040601 (2013).
- [89] M. Esposito and G. Schaller, Stochastic thermodynamics for feedback-controlled systems, *Europhysics Letters* **99**, 30003 (2012).
- [90] B. Annby-Andersson, F. Bakhshinezhad, D. Bhattacharyya, G. De Sousa, C. Jarzynski, P. Samuelsson, and P. P. Potts, Quantum fokker-planck master equation for continuous feedback control, *Phys. Rev. Lett.* **129**, 050401 (2022).
- [91] B. Annby-Andersson, D. Bhattacharyya, P. Bakhshinezhad, D. Holst, G. De Sousa, C. Jarzynski, P. Samuelsson, and P. P. Potts, Maxwell's demon across the quantum-to-classical transition, *Phys. Rev. Res.* **6**, 043216 (2024).
- [92] A. Kutvonen, T. Sagawa, and T. Ala-Nissila, Thermodynamics of information exchange between two coupled quantum dots, *Phys. Rev. E* **93**, 032147 (2016).
- [93] K. Ptaszyński and M. Esposito, Thermodynamics of quantum information flows, *Phys. Rev. Lett.* **122**, 150603 (2019).
- [94] A. J. Leggett, S. Chakravarty, A. T. Dorsey, M. P. A. Fisher, A. Garg, and W. Zwerger, Dynamics of the dissipative two-state system, *Reviews of Modern Physics* **59**, 1 (1987).
- [95] U. Weiss, *quantum dissipative systems* (world scientific, 2012).
- [96] B. K. Agarwalla and D. Segal, Energy current and its statistics in the nonequilibrium spin-boson model: Majorana fermion representation, *New Journal of Physics* **19**, 043030 (2017).
- [97] P. Strasberg, G. Schaller, T. Brandes, and M. Esposito, Quantum and information thermodynamics: A unifying framework based on repeated interactions, *Physical Review X* **7**, 021003 (2017).
- [98] D. Gelbwaser-Klimovsky and G. Kurizki, Heat-machine control by quantum-state preparation: From quantum engines to refrigerators, *Phys. Rev. E* **90**, 022102 (2014).
- [99] D. Segal, Heat flow in nonlinear molecular junctions: Master equation analysis, *Physical Review B* **73**, 205415 (2006).

- [100] A. O. Caldeira and A. J. Leggett, Influence of dissipation on quantum tunneling in macroscopic systems, *Phys. Rev. Lett.* **46**, 211 (1981).
- [101] A. O. Caldeira and A. J. Leggett, Path integral approach to quantum brownian motion, *Physica A* **121**, 587 (1983).
- [102] A. J. Leggett, S. Chakravarty, A. T. Dorsey, M. P. A. Fisher, A. Garg, and W. Zwerger, Dynamics of the dissipative two-state system, *Rev. Mod. Phys.* **59**, 1 (1987).
- [103] R. Kosloff and A. Levy, Quantum heat engines and refrigerators: Continuous devices, *Annu. Rev. Phys. Chem.* **65**, 365 (2014).
- [104] N. Gupt, S. Bhattacharyya, and A. Ghosh, Statistical generalization of regenerative bosonic and fermionic stirling cycles, *Phys. Rev. E* **104**, 054130 (2021).
- [105] S. Kumar, N. Gupt, S. Ghosh, and A. Ghosh, Introduction to quantum thermodynamic cycles, *Journal of Chemical Sciences* **135**, 36 (2023).
- [106] A. Bhardwaj, J. Kaur, M. Wuest, and F. Wuest, In situ click chemistry generation of cyclooxygenase-2 inhibitors, *Nature Communications* **8**, 1 (2017).
- [107] A. Levy and R. Kosloff, Quantum absorption refrigerator, *Phys. Rev. Lett.* **108**, 070604 (2012).
- [108] P. P. Hofer, M. Perarnau-Llobet, J. B. Brask, R. Silva, M. Huber, and N. Brunner, Autonomous quantum refrigerator in a circuit qed architecture based on a josephson junction, *Phys. Rev. B* **94**, 235420 (2016).
- [109] J. Chen, Y. Wang, J. Chen, and S. Su, Optimal figure of merit of low-dissipation quantum refrigerators, *Physical Review E* **107**, 044118 (2023).
- [110] A. Bhattacharyya, A. Ghoshal, and U. Sen, Transient effects in quantum refrigerators with finite environments, *Physical Review A* **111**, 012209 (2025).
- [111] N. Li, J. Ren, L. Wang, G. Zhang, P. Hänggi, and B. Li, Colloquium: Phononics: Manipulating heat flow with electronic analogs and beyond, *Rev. Mod. Phys.* **84**, 1045 (2012).
- [112] R. Sánchez, B. Sothmann, and A. N. Jordan, Heat diode and engine based on quantum hall edge states, *New Journal of Physics* **17**, 075006 (2015).
- [113] B. Li, L. Wang, and G. Casati, Thermal diode: Rectification of heat flux, *Phys. Rev. Lett.* **93**, 184301 (2004).
- [114] R. Scheibner, M. König, D. Reuter, A. D. Wieck, C. Gould, H. Buhmann, and L. W. Molenkamp, Quantum dot as thermal rectifier, *New Journal of Physics* **10**, 083016 (2008).
- [115] J. Ordonez-Miranda, Y. Ezzahri, and K. Joulain, Quantum thermal diode based on two interacting spinlike systems under different excitations, *Phys. Rev. E* **95**, 022128 (2017).
- [116] C. Wang, D. Xu, H. Liu, and X. Gao, Thermal rectification and heat amplification in a nonequilibrium v-type three-level system, *Physical Review E* **99**, 042102 (2019).
- [117] N. Kalantar, B. K. Agarwalla, and D. Segal, Harmonic chains and the thermal diode effect, *Phys. Rev. E* **103**, 052130 (2021).
- [118] A. Marcos-Vicioso, C. López-Jurado, M. Ruiz-Garcia, and R. Sánchez, Thermal rectification with interacting electronic channels: Exploiting degeneracy, quantum superpositions, and interference, *Phys. Rev. B* **98**, 035414 (2018).
- [119] M. Terraneo, M. Peyrard, and G. Casati, Controlling the energy flow in nonlinear lattices: A model for a thermal rectifier, *Phys. Rev. Lett.* **88**, 094302 (2002).
- [120] L. Neumeier, M. Leib, and M. J. Hartmann, Single-photon transistor in circuit quantum electrodynamics, *Phys. Rev. Lett.* **111**, 063601 (2013).
- [121] K. Joulain, J. Drevillon, Y. Ezzahri, and J. Ordonez-Miranda, Quantum thermal transistor, *Phys. Rev. Lett.* **116**, 200601 (2016).
- [122] B.-q. Guo, T. Liu, and C.-s. Yu, Quantum thermal transistor based on qubit-qutrit coupling, *Physical Review E* **98**, 022118 (2018).
- [123] R. T. Wijsekara, S. D. Gunapala, and M. Premaratne, Darlington pair of quantum thermal transistors, *Phys. Rev. B* **104**, 045405 (2021).
- [124] U. N. Ekanayake, S. D. Gunapala, and M. Premaratne, Stochastic model of noise for a quantum thermal transistor, *Physical Review B* **108**, 235421 (2023).
- [125] M. Büttiker, Four-terminal phase-coherent conductance, *Physical Review Letters* **57**, 1761 (1986).
- [126] P. Strasberg, *Quantum Stochastic Thermodynamics: Foundations and Selected Applications* (Oxford University Press, 2022).
- [127] S. Dorsch, A. Svilans, M. Josefsson, B. Goldoizian, M. Kumar, C. Thelander, A. Wacker, and A. Burke, Heat driven transport in serial double quantum dot devices, *Nano Letters* **21**, 988 (2021), pMID: 33459021, <https://doi.org/10.1021/acs.nanolett.0c04017>.
- [128] Y. Zhang and G. Chen, Thermoelectric effects in serially coupled quantum dots, *Scientific Reports* **5**, 16050 (2015).
- [129] T. Brandes, Coherent and collective quantum optical effects in mesoscopic systems, *Physics Reports* **408**, 315 (2005).
- [130] F. Chi, J. Zheng, and K. Zhang, Thermoelectric properties of serially coupled quantum dots, *Nanoscale* **8**, 15927 (2016).
- [131] Y. Zhang, S. Wang, W. Li, and M. Yue, Inverse current induced thermoelectric conversion in a parallel-coupled double quantum dot system, *Physica Scripta* **98**, 105245 (2023).
- [132] A. Ghosh, S. S. Sinha, and D. S. Ray, Canonical formulation of quantum dissipation and noise in a generalized spin bath, *Phys. Rev. E* **86**, 011122 (2012).
- [133] A. Ghosh, S. S. Sinha, and D. S. Ray, Dissipation in a spin bath: Thermally induced coherent intensity and spectral splitting, *Phys. Rev. E* **83**, 061154 (2011).
- [134] A. Ghosh, S. S. Sinha, and D. S. Ray, Fermionic oscillator in a fermionic bath, *Phys. Rev. E* **86**, 011138 (2012).
- [135] L. Wang, Z. Wang, C. Wang, and J. Ren, Cycle flux ranking of network analysis in quantum thermal devices, *Phys. Rev. Lett.* **128**, 067701 (2022).
- [136] E. Pyurbeeva and R. Kosloff, Quantum dot thermal machines—a guide to engineering, *Entropy* **28**, 10.3390/e28010002 (2026).
- [137] Y. Zhang and Z. Xie, Inverse currents in coulomb-coupled quantum dots, *Phys. Rev. E* **104**, 064142 (2021).
- [138] L. Tesser, B. Bhandari, P. A. Erdman, E. Paladino, R. Fazio, and F. Taddei, Heat rectification through single and coupled quantum dots, *New Journal of Physics* **24**, 035001 (2022).
- [139] G. T. Landi and M. Paternostro, Irreversible entropy production: From classical to quantum, *Rev. Mod. Phys.* **93**, 035008 (2021).

- [140] M. Esposito, K. Lindenberg, and C. V. den Broeck, Entropy production as correlation between system and reservoir, *New Journal of Physics* **12**, 013013 (2010).
- [141] N. Walldorf, A.-P. Jauho, and K. Kaasbjerg, Thermoelectrics in coulomb-coupled quantum dots: Cotunneling and energy-dependent lead couplings, *Phys. Rev. B* **96**, 115415 (2017).
- [142] R. S. Whitney, R. Sánchez, and J. Splettstoesser, Quantum thermodynamics of nanoscale thermoelectrics and electronic devices, in *Thermodynamics in the Quantum Regime: Fundamental Aspects and New Directions*, edited by F. Binder, L. A. Correa, C. Gogolin, J. Anders, and G. Adesso (Springer International Publishing, Cham, 2018) pp. 175–206.
- [143] F. J. DiSalvo, Thermoelectric cooling and power generation, *Science* **285**, 703 (1999).
- [144] C. Timm, Gauge theory for the rate equations: Electro-dynamics on a network, *Phys. Rev. Lett.* **98**, 070604 (2007).
- [145] M. Walschaers, J. F.-d.-C. Diaz, R. Mulet, and A. Buchleitner, Optimally designed quantum transport across disordered networks, *Phys. Rev. Lett.* **111**, 180601 (2013).
- [146] R. S. Whitney, R. Sánchez, F. Haupt, and J. Splettstoesser, Thermoelectricity without absorbing energy from the heat sources, *Physica E: Low-dimensional Systems and Nanostructures* **75**, 257 (2016).
- [147] T. Werlang, M. A. Marchiori, M. F. Cornelio, and D. Valente, Optimal rectification in the ultrastrong coupling regime, *Phys. Rev. E* **89**, 062109 (2014).
- [148] Y. Zhang, X. Zhang, Z. Ye, G. Lin, and J. Chen, Three-terminal quantum-dot thermal management devices, *Applied Physics Letters* **110**, 153501 (2017).
- [149] A. A. Aligia, D. P. Daroca, L. Arrachea, and P. Roura-Bas, Heat current across a capacitively coupled double quantum dot, *Phys. Rev. B* **101**, 075417 (2020).
- [150] M. Esposito, N. Kumar, K. Lindenberg, and C. Van den Broeck, Stochastically driven single-level quantum dot: A nanoscale finite-time thermodynamic machine and its various operational modes, *Phys. Rev. E* **85**, 031117 (2012).
- [151] B. Dutta, J. T. Peltonen, D. S. Antonenko, M. Meschke, M. A. Skvortsov, B. Kubala, J. König, C. B. Winkelmann, H. Courtois, and J. P. Pekola, Thermal conductance of a single-electron transistor, *Phys. Rev. Lett.* **119**, 077701 (2017).
- [152] B. Dutta, D. Majidi, N. W. Talarico, N. Lo Gullo, H. Courtois, and C. B. Winkelmann, Single-quantum-dot heat valve, *Phys. Rev. Lett.* **125**, 237701 (2020).
- [153] T. Ruokola and T. Ojanen, Single-electron heat diode: Asymmetric heat transport between electronic reservoirs through coulomb islands, *Phys. Rev. B* **83**, 241404 (2011).
- [154] Y. Zhang, Z. Yang, X. Zhang, B. Lin, G. Lin, and J. Chen, Coulomb-coupled quantum-dot thermal transistors, *EPL (Europhysics Letters)* **122**, 17002 (2018).
- [155] G. Benenti, G. Casati, K. Saito, and R. S. Whitney, fundamental aspects of steady-state conversion of heat to work at the nanoscale, *physics reports* **694**, 1 (2017).
- [156] D. Perez Daroca, P. Roura-Bas, and A. A. Aligia, Role of asymmetry in thermoelectric properties of a double quantum dot out of equilibrium, *Phys. Rev. B* **111**, 045134 (2025).
- [157] A. Hamo, A. Benyamini, I. Shapir, I. Khivrich, J. Waissman, K. Kaasbjerg, Y. Oreg, F. von Oppen, and S. Ilani, Electron attraction mediated by coulomb repulsion, *Nature* **535**, 395 (2016).
- [158] S. M. Tabatabaei, Charge-kondo effect mediated by repulsive interactions, *Phys. Rev. B* **97**, 235131 (2018).
- [159] W. A. Little, Possibility of synthesizing an organic superconductor, *Physical Review* **134**, A1416 (1964).
- [160] G. E. D. K. Prawiroatmodjo, M. Leijnse, F. Trier, Y. Chen, D. V. Christensen, M. von Soosten, N. Pryds, and T. S. Jespersen, Transport and excitations in a negative-u quantum dot at the laalo<sub>3</sub>/srtio<sub>3</sub> interface, *Nature Communications* **8**, 395 (2017).
- [161] G. Benenti, G. Casati, F. Marchesoni, and J. Wang, Autonomous circular heat engine, *Phys. Rev. E* **106**, 044104 (2022).
- [162] J. L. Mateos, Chaotic transport and current reversal in deterministic ratchets, *Physical Review Letters* **84**, 258 (2000).
- [163] S. Kohler, T. Dittrich, and P. Hänggi, Floquet-markovian description of quantum transport, *Physical Review E* **72**, 016124 (2005).

### Appendix A: Derivation of the Lindblad Master Equation for general Quantum Dot–Fermionic Reservoir Model

The dynamical evolution of the system is described using the quantum master equation formulated in the interaction picture. The tunneling Hamiltonian between  $\alpha$ -th QD, and a  $\lambda$ -th bath, introduced in the main text [cf. Eq. (6)], defined as

$$H_T^\lambda \equiv H_T^{\alpha\lambda} = \hbar \sum_k [t_k^{\alpha\lambda} c_{\lambda k}^\dagger d_\alpha + t_k^{\alpha\lambda*} d_\alpha^\dagger c_{\lambda k}]. \quad (\text{A1})$$

Hence, the total tunneling Hamiltonian between the system and the baths can be defined as,  $H_T = \sum_\lambda H_T^\lambda$ . To derive the quantum master equation, we start with the von Neumann equation for the total density operator  $\rho_{\text{tot}}(t)$  in the interaction picture,

$$\frac{d}{dt} \rho_{\text{tot}}(t) = -\frac{i}{\hbar} [H_T(t), \rho_{\text{tot}}(t)]. \quad (\text{A2})$$

Integrating Eq. (A2) and tracing the degrees of freedom of the reservoir, we find

$$\frac{d}{dt}\rho_s(t) = \frac{1}{(i\hbar)^2} \int_0^t dt' \text{Tr}_\lambda \left[ H_T(t), [H_T(t-t'), \rho_{\text{tot}}(t')] \right], \quad (\text{A3})$$

where  $\rho_s(t) = \text{Tr}_\lambda \{\rho_{\text{tot}}(t)\}$  is the reduced system density operator. We further assume  $\text{Tr}_\lambda [H_T(t), \rho_{\text{tot}}(0)] = 0$ . Under the Born-Markov approximation and initially uncorrelated system-bath states, Eq. (A3) can be rewritten as [74, 80, 83]

$$\dot{\rho}_s(t) = \frac{1}{(i\hbar)^2} \sum_{\lambda, \lambda'} \int_0^\infty dt' \text{Tr}_\lambda \left[ H_T^\lambda(t), [H_T^{\lambda'}(t-t'), \rho_s(t) \otimes \prod_\lambda \rho_\lambda] \right]. \quad (\text{A4})$$

We assume that  $\rho_\lambda$  is the initial equilibrium density matrix of the  $\lambda$ -th bath and we use the fact that  $\text{Tr}_\lambda \{c_\lambda(t)\rho_\lambda\} = 0 = \text{Tr}_\lambda \{c_\lambda^\dagger(t)\rho_\lambda\}$  and  $\text{Tr}_\lambda \{[H_T^\lambda(t), [H_T^{\lambda'}(t-t'), \rho_s(t) \otimes \prod_\lambda \rho_\lambda]]\} = 0; \lambda \neq \lambda'$ . Here,  $\text{Tr}_\lambda$  refers to the trace over each bath degrees of freedom and  $\text{Tr}_\lambda \{\rho_{\text{tot}}(t)\} = \rho_s(t)$ , being the reduced density operator of the system. We further assume that  $\text{Tr}_\lambda [H_T(t), \rho_{\text{tot}}(0)] = 0$ . Finally, eliminating the high-frequency oscillating terms by the standard procedure of secular approximation, we arrive at the Lindblad master equation (LME) of the following form

$$\dot{\rho}_s(t) = \sum_\lambda \mathcal{L}_\lambda[\rho_s(t)], \quad (\text{A5})$$

where the Lindblad superoperator  $\mathcal{L}_\lambda$  is given by

$$\begin{aligned} \mathcal{L}_\lambda[\rho_s] = & \sum_{\omega_\alpha > 0} \mathcal{G}_\lambda(\omega_\alpha) \left[ d_\alpha^\dagger(\omega_\alpha) \rho_s d_\alpha(\omega_\alpha) - \frac{1}{2} \{ \rho_s, d_\alpha(\omega_\alpha) d_\alpha^\dagger(\omega_\alpha) \} \right] \\ & + \mathcal{G}_\lambda(-\omega_\alpha) \left[ d_\alpha(\omega_\alpha) \rho_s d_\alpha^\dagger(\omega_\alpha) - \frac{1}{2} \{ \rho_s, d_\alpha^\dagger(\omega_\alpha) d_\alpha(\omega_\alpha) \} \right]. \end{aligned} \quad (\text{A6})$$

Here, the interaction-picture system and bath operators are defined as

$$d_\alpha(t) = \sum_{\omega_{ij} > 0} e^{-i\omega_{ij}t/\hbar} d_\alpha(\omega_{ij}), \quad c_{\lambda k}(t) = e^{-i(\epsilon_k^\lambda - \mu_\lambda)t/\hbar} c_{\lambda k}, \quad (\text{A7})$$

where,  $\omega_{ij}$  is the transition energy between eigenstates  $|\mathbb{i}\rangle$  and  $|\mathbb{j}\rangle$ .  $\mathcal{G}_\lambda(\pm\omega_\alpha) = \gamma_\lambda(\omega_\alpha) f_\lambda^\pm(\omega_\alpha)$ , is the temperature-dependent bath spectral functions, where  $\gamma_\lambda(\omega_\alpha) = 2\pi \sum_k |t_k^{\alpha\lambda}|^2 \delta(\omega_\alpha - \epsilon_k^\lambda)$ . denotes the bare tunnelling rate between reservoir  $\lambda$  and QD $_\alpha$ . The functions  $f_\lambda^\pm(\omega_{ij})$  represent the Fermi-Dirac distribution functions, corresponding to transitions between  $|\mathbb{i}\rangle \rightarrow |\mathbb{j}\rangle$ .

## Appendix B: Derivation of the Steady-State Currents

We assume that the system is initially prepared in equilibrium, i.e.,  $\rho_s(0) = \rho_s^{\text{eq}}$  and the equilibrium density operator of the system is [126]

$$\rho_s^{\text{eq}} = \frac{e^{-\bar{\beta}(H_s - \bar{\mu}\mathcal{N})}}{\mathcal{Z}(\bar{\beta}, \bar{\mu})}, \quad (\text{B1})$$

where the grand-canonical partition function is given by

$$\mathcal{Z}(\bar{\beta}, \bar{\mu}) = \text{Tr} \left[ e^{-\bar{\beta}(H_s - \bar{\mu}\mathcal{N})} \right].$$

Here,  $\bar{\beta} = \sum_\lambda \beta_\lambda$ ,  $\bar{\mu} = \sum_\lambda \mu_\lambda$ , are effective thermodynamic parameters in the presence of multiple reservoirs. Due to interaction with the reservoirs, the system evolves to a time-dependent state  $\rho_s(t)$ , which deviates from equilibrium by an infinitesimally small amount,  $\delta\rho_s(t) = \rho_s(t) - \rho_s(0) = \mathcal{O}(\xi)$ , where  $\xi$  being an small expansion parameter. As long as the system remains close to equilibrium, the von-Neumann entropy is identified with the thermodynamic entropy,

$$\mathcal{S}_s(t) = -k_B \text{Tr}_s[\rho_s(t) \ln \rho_s(t)]. \quad (\text{B2})$$

Following Ref. [126] and keeping terms up to first order in  $\xi$ , the change in entropy is given by

$$\begin{aligned}\Delta\mathcal{S}_s(t) &= \mathcal{S}_s(t) - \mathcal{S}_s(0) \simeq -k_B \text{Tr}_s[\delta\rho_s(t) \ln \rho_s^{\text{eq}}] \\ &= k_B\beta \text{Tr}_s[\delta\rho_s(t)H_s] - k_B\beta\mu \text{Tr}_s[\delta\rho_s(t)\mathcal{N}].\end{aligned}\quad (\text{B3})$$

In the absence of mechanical work, the entropy change is given by

$$\Delta Q = \Delta E - \mu\Delta N, \quad \Delta S = k_B\beta \Delta E - k_B\beta\mu \Delta N. \quad (\text{B4})$$

A comparison between Eqs. (B3) and (B4), yields

$$\Delta E = \text{Tr}_s[\delta\rho_s(t)H_s], \quad \Delta N = \text{Tr}_s[\delta\rho_s(t)\mathcal{N}]. \quad (\text{B5})$$

Since  $H_s$  and  $\mathcal{N}$  are time-independent, energy and particle currents flowing into the system are given by

$$J_E(t) = \text{Tr}_s[\dot{\rho}_s(t)H_s]; \quad J_N(t) = \text{Tr}_s[\dot{\rho}_s(t)\mathcal{N}]. \quad (\text{B6})$$

With the help of the LME,  $\dot{\rho}_s(t) = \sum_\lambda \mathcal{L}_\lambda[\rho_s(t)]$ , the currents can be expressed as

$$J_E(t) = \sum_\lambda \text{Tr}_s[\mathcal{L}_\lambda[\rho_s(t)]H_s]; \quad J_N(t) = \sum_\lambda \text{Tr}_s[\mathcal{L}_\lambda[\rho_s(t)]\mathcal{N}], \quad (\text{B7})$$

while, the total currents can be decomposed into reservoir-resolved contributions,

$$J_E(t) = \sum_\lambda J_E^\lambda(t); \quad J_N(t) = \sum_\lambda J_N^\lambda(t). \quad (\text{B8})$$

Here,  $J_E^\lambda$  and  $J_N^\lambda$  are taken as positive if energy or particles flow from the reservoir  $\lambda$  into the system. Comparing Eqs. (B7) and (B8), the reservoir-resolved currents are identified as

$$J_E^\lambda(t) = \text{Tr}_s[\mathcal{L}_\lambda[\rho_s(t)]H_s]; \quad J_N^\lambda(t) = \text{Tr}_s[\mathcal{L}_\lambda[\rho_s(t)]\mathcal{N}]. \quad (\text{B9})$$

The heat current is defined using the thermodynamic relation  $J_Q(t) = J_E(t) - \mu J_N(t)$ . Decomposing this relation into reservoir contributions

$$J_Q(t) = \sum_\lambda J_Q^\lambda(t) = \sum_\lambda [J_E^\lambda(t) - \mu_\lambda J_N^\lambda(t)], \quad (\text{B10})$$

yields the reservoir-resolved heat current as

$$J_Q^\lambda(t) = J_E^\lambda(t) - \mu_\lambda J_N^\lambda(t). \quad (\text{B11})$$

At steady state,  $J_Q^\lambda(t)$  becomes time-independent, and Eq. (B11) reduces to

$$J_Q^\lambda = J_E^\lambda - \mu_\lambda J_N^\lambda, \quad (\text{B12})$$

where steady state  $J_E^\lambda$  and  $J_N^\lambda$  are given by

$$J_E^\lambda = \text{Tr}_s[\mathcal{L}_\lambda[\rho_{ss}]H_s]; \quad J_N^\lambda = \text{Tr}_s[\mathcal{L}_\lambda[\rho_{ss}]\mathcal{N}]. \quad (\text{B13})$$